FOAMING OF HIGHLY-CRYSTALLINE PLLA FILMS WITH CO2-PHILIC HYBRID LIQUID CELL NUCLEATORS

A THESIS SUBMITTED TO
THE GRADUATE SCHOOL OF NATURAL AND APPLIED SCIENCES
OF
MIDDLE EAST TECHNICAL UNIVERSITY

BY

YAĞMUR ÇULHACIOĞLU

IN PARTIAL FULFILLMENT OF THE REQUIREMENTS
FOR
THE DEGREE OF MASTER OF SCIENCE
IN
CHEMICAL ENGINEERING

JULY 2019

Approval of the thesis:

FOAMING OF HIGHLY-CRYSTALLINE PLLA FILMS WITH CO2-PHILIC HYBRID LIQUID CELL NUCLEATORS

submitted by **YAĞMUR ÇULHACIOĞLU** in partial fulfillment of the requirements for the degree of **Master of Science in Chemical Engineering Department, Middle East Technical University** by,

Prof. Dr. Halil Kalıpçılar
Dean, Graduate School of **Natural and Applied Sciences** _____

Prof. Dr. Pınar Çalık
Head of Department, **Chemical Engineering** _____

Assoc. Prof. Dr. Çerağ Dilek Hacıhabiboğlu
Supervisor, **Chemical Engineering, METU** _____

Prof. Dr. Nesrin Hasırcı
Co-Supervisor, **Chemistry, METU** _____

Examining Committee Members:

Prof. Dr. Nihal Aydoğan
Chemical Engineering, Hacettepe University _____

Assoc. Prof. Dr. Çerağ Dilek Hacıhabiboğlu
Chemical Engineering, METU _____

Assoc. Prof. Dr. Ali Durmuş
Chemical Engineering, Istanbul University-Cerrahpaşa _____

Assoc. Prof. Dr. Erhan Bat
Chemical Engineering, METU _____

Asst. Prof. Dr. Harun Koku
Chemical Engineering, METU _____

Date: 30.07.2019

I hereby declare that all information in this document has been obtained and presented in accordance with academic rules and ethical conduct. I also declare that, as required by these rules and conduct, I have fully cited and referenced all material and results that are not original to this work.

Name, Surname: Yağmur Çulhacıoğlu

Signature:

ABSTRACT

FOAMING OF HIGHLY-CRYSTALLINE PLLA FILMS WITH CO2-PHILIC HYBRID LIQUID CELL NUCLEATORS

Çulhacıoğlu, Yağmur
Master of Science, Chemical Engineering
Supervisor: Assoc. Prof. Dr. Çerağ Dilek Hacıhabiboğlu
Co-Supervisor: Prof. Dr. Nesrin Hasırcı

July 2019, 76 pages

Supercritical CO_2 ($scCO_2$) foaming of poly($_L$-lactic acid) (P_LLA) composites with CO_2-philic additives was carried out to obtain polymeric matrices as carriers for drug delivery applications. Highly crystalline P_LLA (>45%) generally requires high processing temperatures close to its melting point (~450 K), and pressures about or over 20 MPa for foaming with $scCO_2$. In this study, in order to decrease the saturation temperature and obtain ductile P_LLA films with homogeneously distributed uniform porosity, two different novel CO_2-philic organic-inorganic hybrid liquid POSS (isooctyl POSS and methacrylisooctyl POSS) were used as cell nucleators. Porous thin films were obtained by the solvent-casting of the polymer with these additives even prior to $scCO_2$ foaming of composites. Meanwhile, $scCO_2$ processing of these films at 313 K and 21 MPa, increased the pore density. Also, foaming of highly crystalline P_LLA composite films (>45%) was achieved at low temperature with the help of two novel CO_2-philic components used as cell nucleators. $scCO_2$ processing enhanced the mechanical and thermal properties such as elastic modulus and T_g of the highly-crystalline P_LLA porous films. $scCO_2$ processing of composite films also allowed extraction of almost all cell nucleator from matrices. Drug release studies with a model antibiotic (Ceftriaxone Sodium) showed that the porous films exhibit burst release characteristics, which is suitable for local antibiotic applications.

Keywords: Supercritical Carbon Dioxide Foaming, Poly(L-Lactic Acid), Polyhedral Oligomeric Silsesquioxane, Porous Ductile Films, Drug Release

ÖZ

CO2 İLE UYUMLU HİBRİT SIVI POR İNDÜKLEYİCİ İÇEREN YÜKSEK KRİSTALİNİTEYE SAHİP PLLA FİLMLERİNİN KÖPÜKLEŞTİRİLMESİ

Çulhacıoğlu, Yağmur
Yüksek Lisans, Kimya Mühendisliği
Tez Danışmanı: Doç. Dr. Çerağ Dilek Hacıhabiboğlu
Ortak Tez Danışmanı: Prof. Dr. Nesrin Hasırcı

Temmuz 2019, 76 sayfa

İlaç taşıma uygulamalarında kullanılacak polimerik yapılar eldesi için poli($_L$-laktik asit) (P_LLA)'in CO_2-uyumlu katkı maddeleriyle kompozitleri süperkritik CO_2 ($scCO_2$) ile köpükleştirildi. Yüksek kristalinitedeki P_LLA'nın (>%45), süperkritik CO_2 ile köpükleştirilmesi genellikle erime noktasına yakın yüksek işleme sıcaklıkları (~450 K) ve 20 MPa veya üzeri basınçlar gerektirir. Bu çalışmada, doygunluk sıcaklığını düşürmek, homojen dağılımlı gözeneklere sahip ve esnek P_LLA filmleri elde etmek için, iki farklı CO_2-uyumlu organik-inorganik hibrit sıvı POSS (isooctyl POSS ve methacrylisooctyl POSS) gözenek indükleyici olarak kullanıldı. Kompozitlere $scCO_2$ köpükleştirme işlemi uygulanmadan önce bile, polimerin bu katkı maddeleriyle çözelti dökümünden gözenekli ince filmler elde edildi. Aynı zamanda, bu filmlerin $scCO_2$ ile 313 K ve 21 MPa'da işlenmesi gözenek yoğunluğunu artırdı. Ayrıca kullanılan yeni CO_2-uyumlu gözenek indükleyiciler sayesinde yüksek kristalinitedeki P_LLA kompozit filmlerinin (>45%) köpükleştirilmesi düşük sıcaklıkta gerçekleşti. $scCO_2$ işlemesi yüksek kristaliniteye sahip gözenekli P_LLA filmlerinin elastik modülüs ve T_g gibi mekanik ve termal özelliklerini geliştirdi. Kompozit filmlerin $scCO_2$ ile işlenmesi aynı zamanda gözenek indükleyicilerin büyük kısmının matriks içinden özütlenmesini sağladı. Model antibiyotik (Ceftriaxone Sodium) ile yapılan ilaç

salım çalışmaları, gözenekli filmlerin hızlı salım sergilediği ve lokal antibiyotik uygulamaları için uygun olduğunu gösterdi.

Anahtar Kelimeler: Superkritik Karbondioksit Köpükleşmesi, Poli(L-Laktik Asit), Polihedral Oligomerik Silseskuioksan, Gözenekli Esnek Film, İlaç Salımı

To my beloved family…

ACKNOWLEDGMENTS

I would like to express my deepest appreciation to my supervisor Assoc. Prof. Dr. Çerağ Dilek Hacıhabiboğlu and my co-supervisor Prof. Dr. Nesrin Hasırcı for their guidance, patience, continuous support and encouragement throughout the research.

I would like to thank Dr. Tuğba Endoğan Tanır for her help during drug release studies.

I am thankful for my lovely friends Aslı Karausta, Nisa Erişen, Nur Ber Emerce, Soner Yaşar, Almira Çaldıkoğlu, Berrak Erkmen, Ezgi Yavuzyılmaz, Fatma Şahin, Merve Sarıyer, Seda Sivri, Selin Şahin, Zeynep Karakaş for their help and advice during this study. I would also like to thank my lab-mates Beril Dumanlılar and Merve Özkutlu for their supports and helps throughout my laboratory studies. I would like to express my special thanks and gratitude to Görkem Kızal for his moral support. I am so lucky and blessed to have them in my life.

Last but not the least, I owe a great debt of gratitude to my mom Nergis Çulhacıoğlu, my dad Hüseyin Çulhacıoğlu and my little sister Damla Çulhacıoğlu for their endless love, encouragement, support and being there whenever I need. I never would have made it this far without them.

TABLE OF CONTENTS

LIST OF TABLES

TABLES

LIST OF FIGURES

FIGURES

LIST OF ABBREVIATIONS

ABBREVIATIONS

$scCO_2$	Supercritical CO_2
$\boldsymbol{d_a}$	Average pore diameter (μm)
$\boldsymbol{d_i}$	Pore diameter of the single pore (μm)
DSC	Differential scanning calorimetry
DoE	Design of experiments
EDX	Energy-dispersive X-ray spectroscopy
IPOSS	Isooctyl POSS
IP_LLA	P_LLA-Isooctyl POSS composite film
MPOSS	Methacrylisooctyl POSS
MP_LLA	P_LLA-Methacrylisooctyl POSS composite film
M_w	Molecular weight (g/mol)
$\boldsymbol{\bar{M}_w}$	Average molecular weight (g/mol)
$\boldsymbol{n_i}$	Number of the samples measured
SPOSS	Octatrimethylsiloxy POSS
P_c	Critical pressure
$P_{DL}LA$	Poly($_{DL}$-lactic acid)
PLA	Poly(lactic acid)
P_LLA	Poly($_L$-lactic acid)
PBS	Phosphate buffered saline solution

POSS	Polyhedral oligomeric silsesquioxane
SA	Sugar acetate (β-$_D$-galactose pentaacetate)
SEM	Scanning electron microscopy
SP	Saturation pressure (MPa)
ST	Saturation temperature (K)
$\mathbf{S_{time}}$	Saturation time (hour)
$\mathbf{T_c}$	Critical temperature
$\mathbf{T_g}$	Glass transition temperature (K)
VR	Venting rate (MPa/min)
wt	Weight
$\boldsymbol{w_{P_LLA}}$	The weight fraction of the P_LLA in the sample
$\boldsymbol{X_{Crys}}$	Degree of crystallinity of the sample
$\boldsymbol{\eta_{inh}}$	Inherent viscosity (dL/g)
$\boldsymbol{\Delta H_c}$	Specific cold crystallization enthalpy (J/g)
$\boldsymbol{\Delta H_m}$	Specific melting enthalpy of the sample (J/g)
$\boldsymbol{\Delta H_m^o}$	Specific melting enthalpy of 100% crystalline sample (J/g)

CHAPTER 1

INTRODUCTION

1.1. P_LLA

There is an increasing trend towards replacing petroleum-based polymers with their natural counterparts for their benign nature and biodegradability that leads to decrease in non-biodegradable plastic waste disposal [1–3]. Poly(lactic acid) (PLA) is one of the most promising natural-based polymers that can be replaced with non-biodegradable polymers like polystyrene, polyethylene, poly(ethylene terephthalate) for its thermoplastic processability, adjustable mechanical and thermal properties as well as controllable degradation rate, and most importantly its non-toxic, bio-degradable and bio-compatible nature [2,4–7]. Therefore, PLA can be used in different industries like fiber and textile and as a commodity product like packaging, plastic utensils, sound and thermal insulation, etc. PLA and its blends are also widely used in the production of biomedical devices like drug delivery vehicles, artificial vasculature system, degradable suture, implants, bone fixation devices (plates and screws), and as porous scaffolds for bone tissue engineering applications [8–13]. PLA also is an approved polymer by the US Food and Drug Administration (FDA) in clinical use. Its usage in biomedical applications is expected to increase at least 10 % per year which makes PLA leading polymer in this industry.

Lactic acid, the building block of PLA, can be produced by means of chemical synthesis or bacterial fermentation. In the former method, a racemic mixture of $_L$- and $_D$- isomers is obtained while optically pure $_L$- or $_D$- isomer can be obtained in the fermentation process by selecting the certain type of bacteria [10,14]. However, most of the microorganisms produce $_L$-lactic acid, therefore, in biotechnology and tissue engineering, P_LLA and $P_{DL}LA$ are studied and produced widely [15]. Nowadays, the

fermentation route of production of lactic acid is preferred because of environmental concerns, reduction of usage of petroleum-based resources, low energy, and temperature requirement, cheap raw materials in addition to obtaining optically pure isomers [10,14].

Since PLA is a racemic mixture of $_{L}$- and $_{D}$- isomers, its degradation behavior, mechanical and thermal properties can be monitored by determining the ratio of them. $P_{L}LA$ is an isotactic polymer that has a melting point temperature between 446 and 451 K, glass transition temperature between 323 and 353 K and crystallinity around 37 % [10,16]. Polymerization of a racemic mixture of $_{L}$- and $_{D}$-lactides usually leads to the formation of poly-$_{DL}$-lactide ($P_{DL}LA$) which is amorphous when $_{D}$-isomer is higher than 7% [4,17].

1.1.1. PLA in Biomedical Applications

For biomedical applications, biodegradable polymers have gained great attention due to their advantages over non-biodegradable polymers [10,18]. Usage of biodegradable polymer does not require further operation for removal since they offer long-lasting biocompatibility. PLA is the most promising polymer for this purpose since it provides controllable degradation rate by forming copolymers, also high biocompatibility and good mechanical properties. In addition, it can be produced from renewable sources like corn, sugar cane, etc. Instead of neat PLA, its blends or copolymer with other polymers have been used mostly to obtain the desired features. Since surface characteristic is an important parameter for biomaterials, different surface modification methods such as physical, chemical, plasma, and radiation induced methods are applied to increase the applicability of the polymer matrix [3,10].

PLA is a highly preferred bio-degradable polymer for bone fixation devices (plate, screws, pins, wires, etc.) since it provides high stiffness and strength similar to bone [10,18]. These devices can be used in shoulder, knee, elbow, hand, wrist, pelvis, zygomatic, foot and ankle fractures. Porous PLA scaffolds have been also used to

culture different cell types to use in muscle tissues, bone and cartilage regeneration, cell-based gene therapy for cardiovascular diseases and other treatments of cardiovascular, neurological, and orthopedic conditions, etc. [10].

High crystalline structure and low degradation rate restrict PLA usage as suture [3,10]. For this reason, PLA is copolymerized with polyglycolic acid. On the other hand, for situations that require long retention of strength (ligament and tendon reconstruction, and stents for vascular and urological surgery, etc.) P_LLA fibers are desired. P_LLA matrices are also used as drug delivery systems.

1.1.2. PLA in Drug Delivery

Having biodegradability, biocompatibility, low toxicology and good encapsulation capability, biodegradable polymers like PLA have been used as drug release systems [3,18]. Generally, the release of the drug occurs by the erosion of the polymer matrix by penetrating water (hydrolytic degradation). Polymer breaks down to its monomer units connected with ester bonds. Diffusion and swelling of the polymer are other methods for drug release. Encapsulation of a variety of chemicals and drugs (such as AG-1295 (for restenosis), oridonin (for esophageal and hepatic carcinoma), savoxepine (as antipsychotic), progesterone (hormones) and BSA (protein), etc.) were conducted by using PLA and its polymer blends in the form of nanoparticles [18]. Different production methods have been used to produce drug-loaded nanoparticles like salting out, solvent displacement, emulsion solvent diffusion and solvent evaporation. Film type PLA is also used in drug delivery systems. The first usage of the film type is reported for slow release of narcotic antagonists by Yolles and Colleagues [19,20]. In a study conducted by Krukiewicz *et al*., it was found that drug-loaded PLA films were successful to inhibit repetition of the tumor [21]. There are different types of commercially available PLGA drug delivery systems for cancer treatment. These products are OncoGel® (brain tumor), Zoladex® and Eligard® (breast or prostate cancer).

Since the structure of the tooth pocket permits the insertion of the film type of matrix, their release systems are also suitable for periodontal applications [22]. PerioChip® is one of the commercially available periodontal drug systems that has biodegradable matrix of hydrolyzed gelatin (cross-linked with glutaraldehyde) and ensures the constant release of chlorhexidine up to one week.

1.2. Supercritical CO_2

A fluid can be defined as supercritical when its temperature and pressure are higher than its critical temperature and pressure. In Figure 1.1, the phase diagram of a pure material is given. In the supercritical region, there is no definite phase boundary between the liquid and gas phase, and the fluid at those conditions has properties of both phases [23]. Solvent power and density of the supercritical fluid are similar to liquid phase whereas its mass transfer properties are similar to the gas phase. These properties can be monitored easily by changing temperature and pressure.

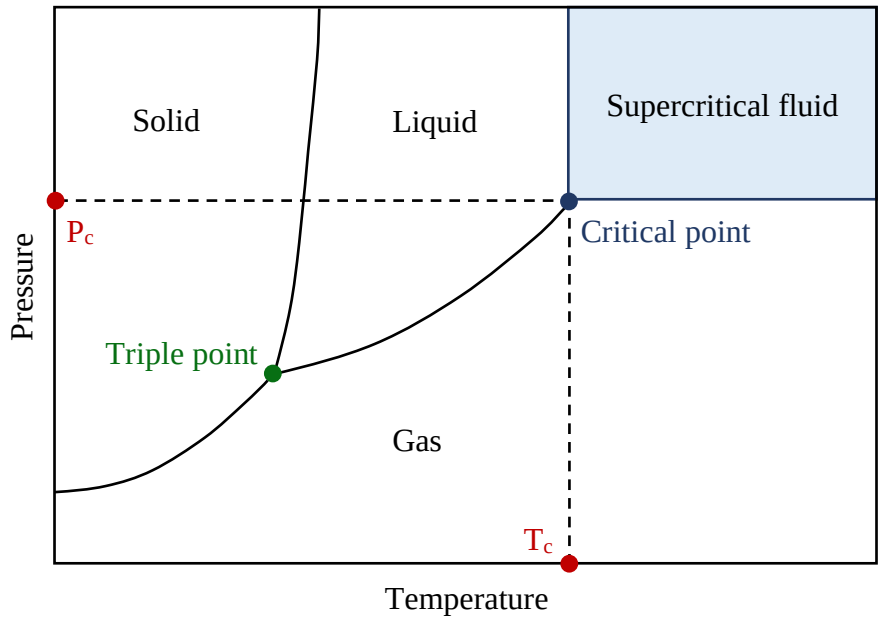

Figure 1.1. Pressure-Temperature diagram of a pure substance

Critical parameters of some solvents are given in Table 1.1. Among all supercritical fluids, $scCO_2$ is the most commonly used solvent for material processing since it offers green processing techniques at mild conditions by eliminating the usage of organic solvents [24–28]. Its lower critical parameters (T_c=304 K, P_c= 7.4 MPa) than other supercritical fluids make it advantageous for processing of thermally sensitive materials. It is also non-toxic, non-flammable, environmentally benign, inert, cheap and abundant in nature. Meanwhile, it is considered as GRAS (Generally Regarded as Safe) solvent. Its extraction is performed simply by venting and the remaining structure is easily obtained dry without any residue or impurity. In addition, CO_2 can be collected and reused so there is no contribution to the greenhouse effect. $scCO_2$ is used for different applications like impregnation, sterilization, and drying, and it can also be used in polymer processing.

Table 1.1. *The critical parameters of some solvents*

Solvents	Critical Temperature (T_c, K)	Critical Pressure (P_c, MPa)
Ammonia	406	11.3
Benzene	562	4.9
Carbon dioxide	*304*	*7.4*
Ethane	305	4.9
Ethylene	283	5.1
Isopropanol	509	4.9
Propane	370	4.3
Propylene	365	4.6
Toluene	593	4.1
Water	647	22.1

1.3. Porous Scaffold Production

Different production techniques, such as thermally induced phase separation, solvent casting-particle leaching, freeze–drying–particle leaching, injection molding, compression molding, electrospinning, wet spinning, foaming, etc. are available to obtain 3D scaffolds for using in biomedical engineering [25,26,28,29]. Some of these techniques are explained below.

1.3.1. Porous Scaffold Production with Solvent Casting-Particle Leaching

In this technique of obtaining porous scaffolds, polymer is dissolved in chloroform or methylene chloride and water-soluble porogen is added to the solution [30–32]. Porogens remain in the polymer matrix as embedded after solvent evaporation by freeze drying, air drying or vacuum drying. Then, the polymer-porogen matrix is immersed in water for the extraction of the porogen. Salt is used generally, but there are examples of usage of gelatin, sugar, starch particles, ammonium chloride in the literature. The porosity of the matrix depends on the porogen amount in the solution whereas pore size is related to the particle size of the used porogen. It was stated that 70 wt % or higher porogen amount resulted in interconnected porous structure. On the other hand, if porogen amount is too high, voids (huge hollows that interrupts the matrix integrity) are formed in the polymer matrix whereas lack of porogen resulted in a closed pore structure. No need for specific equipment in this technique is an advantage. However, the usage of organic solvent restricts its usage.

1.3.2. Porous Scaffold Production with Compression Molding

This technique is very similar to solvent casting particulate leaching method. Polymer powder or granulated polymer is mixed with water-soluble porogen [33]. The polymer mixture is placed in a mold to be pressed between hot plates with high pressure. After obtaining polymer-porogen matrix without an air bubble, the porogen is removed with water immersion of the matrix.

1.3.3. Porous Scaffold Production with Thermally Induced Phase Separation

In thermally induced phase separation technique, a solvent having high boiling point and low molecular weight is mixed with polymer at elevated temperature [31,34]. Then obtained solution is poured into a container that is shaped like the desired structure (sheet, tube vs.). Container is cooled to the solvents' freezing point to induce phase separation. Then polymer matrix solidifies, and porous structure is obtained. The properties of the obtained matrix depend on the solvent amount, cooling rate and temperature reached during cooling. This technique is advantageous since any porous shape can be simply obtained. On the other hand, the matrix has a micropore structure.

1.3.4. Porous Scaffold Production with Electrospinning

This technique is used for nanofiber production. For this method, the polymer solution is placed in a spinneret (like pipette tip) and polymer solution is charged with high voltage power supply [34,35]. From a metallic needle, polymer melt is slowly fed under the electric charge which resulted in a hanging droplet (Taylor cone) in the needle tip. Droplet's surface tension is in equilibrium with the electric field. Tiny jet exits from the droplet if the electric field is high enough to overcome the surface tension. During this ejection of jet, solvent in the jet stream evaporates gradually and nonwoven porous matrix is obtained at the end of the jet stream. Obtained fiber thickness and matrix properties can be controlled by tuning the solvent of the polymer solution, electric field, the distance between the needle and collecting container humidity and temperature. The volatility of the solvent is one of the key parameters. If solvent has low volatility, solvent does not evaporate and fibers will be wet whereas if solvent has high volatility, jet stream solidifies, and fiber does not form. Pores in the fiber surface are affected by humidity since solvent evaporation is related to it. Matrices obtained with technique has high interconnectivity in addition to uniform pore size and distribution.

Besides their advantages, often organic solvents are used during these processes and therefore further drying and purification steps are needed. In addition to these, high temperature is a must for some techniques which is harmful to thermally sensitive materials like bioactive compounds and drugs, and causes loss of activity or degradation of them. Therefore, the $scCO_2$ processing technique of polymers can be an alternative to others since it reduces or eliminates the use of organic solvents and does not need further purification steps like other conventional techniques.

1.3.5. Porous Scaffold Production with Supercritical CO_2

$scCO_2$ can be used as a foaming agent because of its plasticization effect on the polymers with CO_2 affinity [25–29,36,37]. CO_2 dissolution in the polymer matrix increases the chain mobility and cause relaxation because of its plasticization effect that leads to a decrease in the glass transition temperature (T_g) of the matrix. This allows processing of such polymers at temperatures lower than their T_g. After a certain saturation time (S_{time}), decreasing the pressure of the system by simply venting with certain venting rate (VR), decreases the solubility of CO_2 in the polymer. This causes supersaturation with thermodynamic instability which induces nucleation and growth of the bubbles in the polymer matrix. As the same time with the decreasing pressure, T_g of the polymer increases. After some point, T_g would be higher than process temperature which is the point of the porous structure of the polymer is obtained in a glassy state. Saturation temperature, saturation pressure, venting rate of CO_2 and concentration of the CO_2 in the polymer are important parameters in $scCO_2$ foaming processing of polymers [38,39]. In this field, the term of "saturation" is a common world since in supercritical processes polymer matrix come to contact with CO_2 at certain saturation temperature (ST) and saturation pressure (SP) for a certain S_{time} where CO_2 is allowed to diffuse into the matrix and become saturated.

CHAPTER 2

LITERATURE REVIEW

2.1. Literature Study on PLA and $scCO_2$ System

2.1.1. The Solubility of $scCO_2$ in $P_{DL}LA$ and P_LLA

In the polymer foaming processes, ST, SP, S_{time} and VR are the adjustable parameters whereas CO_2 concentration in the polymer matrix depends on the solubility of CO_2 in the matrix. The solubility of the CO_2 in the polymer depends on molecular structure and crystallinity [40].

There are some studies in the literature focused on the solubility of $scCO_2$ in PLA having different crystallinity, $_D$- content and molecular weight. Chemical structure of P_LLA is given in Figure 2.1. One of the studies shows that amorphous $P_{DL}LA$ (with 20 % $_D$- content) had higher CO_2 solubility than semi-crystalline $P_{DL}LA$ (with 2 % $_D$- content) indicating that crystallinity of the polymer is an important property for solubility of a gas in the matrix [41]. CO_2 solubility in the polymer was studied by using different molecular weights of $P_{DL}LA$ (15,000 and 52,000 g/mol) at 308 K and pressure up to 20 MPa. At 20 MPa, $scCO_2$ solubility was found to be around 35 wt % in both polymers, showing that the molecular weight in the studied range did not affect the solubility [42]. In another study, CO_2 solubility in P_LLA with a molecular weight of 42,000 g/mol and crystallinity of 54 % was found to be about 39 wt % at 313 K and 20 MPa [43]. Jinpeng *et al.* determined that the solubility increased with decreasing temperature and increasing pressure, and also measured 17 wt % of CO_2 solubility at 313 K and 20 MPa, which was the highest that they measured in P_LLA films with a molecular weight of 11,300 g/mol (any crystallinity value was not given) [44]. The difference between the solubility values in the last two mentioned study may result

from different crystallinity values since their solubility data is given for similar conditions and in that range, molecular weight of the polymer generally does not have a significant effect on solubility.

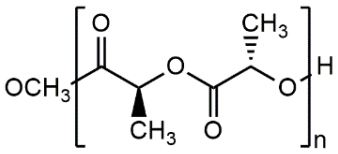

Figure 2.1. Molecular structure of P_LLA

2.1.2. $scCO_2$ Foaming of PLA

2.1.2.1. $scCO_2$ Foaming of P_LLA without Additive

Even though P_LLA is widely used in both industrial and biomedical applications because of its preferable mechanical properties and long degradation time than $P_{DL}LA$, $scCO_2$ foaming applications are mainly concentrated on $P_{DL}LA$ due to its low energy requirements in the process since low temperatures and pressures are enough for obtaining highly porous structures. This is because of different crystallinity values of the P_LLA and $P_{DL}LA$ since it has been reported that foaming of semi-crystalline polymers requires higher process temperatures compared with amorphous ones [45]. Liao *et al*. observed this behavior in semi-crystalline P_LLA [46]. They used P_LLA with different crystallinity values to foam. Foaming was performed at temperatures between 323 and 472 K and pressures between 2.1 and 5.5 MPa. Even if the crystalline phase can act as a nucleation agent in semi-crystalline polymers [47], there was no pore formation at 323 K if the crystallinity was higher than 30 %, and at higher temperatures only some gaps were obtained in the polymer structure. This is a consequence of increased rigidity and stiffness of the matrix with higher crystallinity, which reduces

the solubility of CO_2. Therefore, it is hard to obtain detectable pores at low temperatures.

Kiran reported the minimum conditions to induce foaming of P_LLA with a molecular weight of 127,000 g/mol and 100% $_L$- content as 20 MPa and at least 391 K, and 41 MPa and at least 353 K indicating that at lower pressures, higher temperatures are needed [17]. Study about CO_2 sorption of P_LLA studied by Jinpeng *et al.* supports Kiran's study; they did not observe any porous structure on pure P_LLA films with a molecular weight of 11,300 g/mol processed at 313 K and 20 MPa [44]. In another study in P_LLA with a molecular weight of 350,000 g/mol and crystallinity of 80 %, a porous structure was not observed after 24 hours of processing with $scCO_2$ at 393 K and 12 MPa [48]. On the other hand, $P_{DL}LA$ having molecular weights of 57,000, 25,700 and 15,000 were foamed at 308 K and 23 MPa and their average porosity was stated as 70% [27]. As it can be seen at conditions that P_LLA can not induce pore formation, $P_{DL}LA$ can be foamed easily.

2.1.2.2. $scCO_2$ Foaming of P_LLA with Additive

2.1.2.2.1 $scCO_2$ Foaming of P_LLA with non-CO_2-philic Additive

There are several studies on foaming of P_LLA with an additive for different purposes but mostly to improve the mechanical behavior of the polymer. Mathieu *et al*. used hydroxyapatite (HAp) and β-tricalcium phosphate (β-TCP) in the P_LLA matrix with 5 wt % in order to enhance cell attachment and bone regeneration [49]. The saturation temperature, pressure, and time were kept constant at 468 K, 10-25 MPa and 10 minutes, respectively, while depressurization rates were varied. The presence of the fillers improved the compressive moduli and compressive strengths of the foamed samples about two times from 100 MPa and 3 MPa to 200 MPa and 6 MPa, respectively. The foamed structures of composites had more heterogeneous pore distributions and more closed pore structures compared to processed neat porous P_LLA samples. In another study, on the other hand, Delabarde *et al.*, reported that

addition of the HAp nanoparticles (up to 4.17 volume %) resulted in homogeneous structures with smaller pore size (decreased from 0.5–1 mm to 150–400 μm) and open pore structures compared to pristine samples [50], while there was no significant effect of the supercritical processing or presence of filler on the mechanical properties. Georgiou *et al*. used phosphate glass as filler at 5 and 10 wt % in the P_LLA matrix, and found that it did not enhance the compressive modulus of the samples foamed with application of $scCO_2$ at 468 K and pressures between 15 and 25 MPa, while smaller pores were observed in the composites compared to neat P_LLA [51]. The study also revealed that T_g of the samples increased after $scCO_2$ processing (with an average T_g of 342 K) compared to unprocessed samples (with an average T_g of 334 K).

2.1.2.2.2 $scCO_2$ Foaming of P_LLA with CO_2-philic Additive

It is known that nano/micro-particles in the polymer matrix act as heterogeneous nucleation agent and increases the cell nucleation rate and therefore cell density during $scCO_2$ foaming by lowering free energy barrier [6,52,53]. In addition, the presence of the CO_2-philic components in the polymer matrix increase nucleation sites by both increasing CO_2 amount and introducing new nuclei interface the polymer [54,55]. In literature, it is given that polyhedral oligomeric silsesquioxane (POSS) which is an organic-inorganic hybrid molecule, is a non-toxic (or has quite low toxicity) and cytocompatible material [56]. Also, usage of POSS in polymers as a filler generally reinforces the matrix by enhancing their thermal, physical and mechanical properties. Because of these reasons, POSS molecules and its blends with polymers have been widely used in biomedical areas such as drug delivery [57–59], dental applications [60–62], biosensors [63], cardiovascular implants [64] and tissue engineering (small intestine, liver and cartilage) [65–67]. Therefore, in the previous foaming study conducted in our laboratory, POSS compounds were used as cell nucleating chemicals in the P_LLA matrix [38]. A highly CO_2-soluble additive, trifluoropropyl polyhedral oligomeric silsesquioxane (TFPOSS) [68] was used as a heterogeneous nucleation agent in order to foam a highly crystalline P_LLA having 45.7 % crystallinity and 100,000 g/mol

molecular weight at low temperature and pressure. Increasing the affinity between the polymer matrix and $scCO_2$, foaming of the polymer as succeeded at 313 K and 20.7 MPa for the first time in the literature. However, obtained porous matrices were rigid and fragile, and pore distributions were not homogeneous in the matrix. The inhomogeneous distribution was attributed to the poor dispersion of the TFPOSS particles in the solvent-cast polymer. Meanwhile, neat polymer matrix or polymer composite with non-CO_2-philic type additive, octamethyl POSS [69], did not form any porous structure when processed under the same conditions.

2.2. The Solubility of Used Additives in CO_2

2.2.1. β-D Galactose Pentaacetate

β-$_D$ galactose pentaacetate or sugar acetate (SA) was chosen as an additive in the polymer matrix for nucleation of the bubbles in $scCO_2$ process since it has a benign nature and high solubility in CO_2. The chemical formula of β-$_D$ galactose pentaacetate is given in Figure 2.2(a).

Potluri *et al*. studied the solubility of acetylated sugar derivatives including SA in $scCO_2$ [70]. They observed solubility of SA is about 25 wt % at 10.6 MPa and 313 K. They also stated that, after depressurization of CO_2, remaining SA has a porous form. Another work on the solubility of SA was carried out by Raveendran *et al*. and they reported similar results [71]. The solubility of SA was found as 23.6 wt % at 313 K and 11.1 MPa. In their phase behavior study, Dilek *et al*. found 25.9 wt % solubility of SA at 11.4 MPa and 313 K [72]. These studies are carried out almost under the similar conditions and resulted in approximately 25 wt % solubility of SA in CO_2.

2.2.2. Polyhedral Oligomeric Silsesquioxane (POSS)

POSS which is an organic-inorganic hybrid molecule was selected as a cell nucleator because it is non-toxic or has quite low toxicity and has cytocompatible features [56]. It has cage-like and 3-dimensional molecular structure and generally defined as $R_nSi_nO_{1.5n}$. The framework of the POSS consists of silicone and oxygen atom and it's

covered with other functional groups (R). Usage of POSS in polymers as a filler generally reinforces the matrix by enhancing their thermal and mechanical properties. Because of these reasons, polymer composites with POSS molecules have been widely used in biomedical applications such as drug delivery [57–59], dental applications [60–62], biosensors [63], cardiovascular implants [64] and tissue engineering (small intestine, liver and cartilage) [65–67].

The following studies of different POSS types are about their solubility in CO_2, without using any polymeric matrix.

2.2.2.1. Octatrimethylsiloxy POSS (SPOSS)

Octatrimethylsiloxy POSS- CO_2 binary system was studied by Demirtas *et al.* and they obtained solid-vapor equilibrium with a temperature range of 308-328 K [73]. The highest solubility obtained at 328 K and 13.4 MPa as 17.6 wt %. In addition to that, the solubility of POSS was found as 15.3 wt % at 313 K and 10.6 MPa. The chemical formula of SPOSS is given in Figure 2.2 (b).

2.2.2.2. Isooctyl POSS (IPOSS)

The solubility of Isooctyl POSS in scCO_2 studied by Kanya *et al.* They found the highest solubility at 308 K and 17.2 MPa as 2 wt % [69]. The chemical formula of IPOSS is given in Figure 2.2(c).

2.2.2.3. Methacrylisooctyl POSS (MPOSS)

Methacrylisooctyl POSS (MPOSS)-CO_2 binary system was studied by Dumanlilar *et al.* [74]. They found the solubility of MPOSS as 4.9 wt % at 313 K and 19.4 MPa. The chemical formula of MPOSS is given in Figure 2.2 (d).

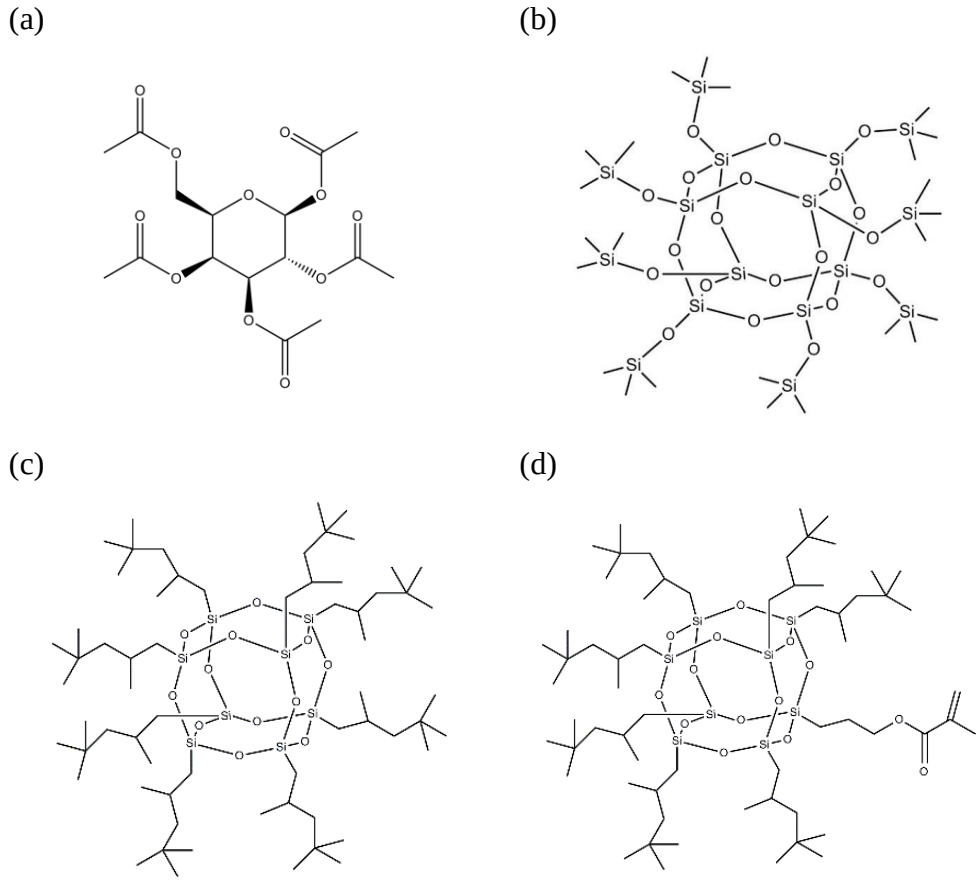

Figure 2.2. Molecular structures of (a) β-$_D$ Galactose Pentaacetate, (b) SPOSS (c) IPOSS, (d) MPOSS

2.3. Aim of this Study

In this work, to improve the foaming performance of the highly crystalline P_LLA and obtain ductile and porous films with homogeneous pore distributions, different nucleating agents were used. Especially two types of CO_2-philic liquid POSS were promising as heterogeneous nucleating agents. One of these molecules is isooctyl POSS (IPOSS) (Figure 2.1(c))[69] which has eight isooctyl substituents bonded to the inorganic cage. The other one is methacrylisooctyl POSS (MPOSS) (Figure 2.1(d))[74] with a molecular structure similar to the previous one except for one methacryl branch

and it has recently been reported as CO_2-philic. The foaming experiments of P_LLA composites with these additives were conducted by using design of experiments (DoE). The morphological, mechanical and thermal properties of the obtained porous films were examined in detail.

CHAPTER 3

EXPERIMENTAL

3.1. Materials

Poly(L-lactic acid) (P_LLA) ($\bar{M}_w$ =80000-100000 g/mol, η_{inh}=1.8 dL/g) was purchased from Polysciences, Inc. (Warrington, USA) in granular form and kept in a desiccator at room temperature. Two liquid polyhedral oligomeric silsesquioxane (POSS) compounds, namely isooctyl POSS (IPOSS) ($(C_8H_{17})_8(SiO_{1.5})_8$, M_w=1322.46 g/mol) and methacrylisooctyl POSS (MPOSS) ($(C_8H_{17})_7(C_7H_{11}O_2)(SiO_{1.5})_8$, M_w=1336.38 g/mol) and a solid one octatrimethylsiloxy POSS (SPOSS) ($(C_8H_4F_3)_8(SiO_{1.5})_8$, Mw=1193.16 g/mol) were provided from Hybridplastics (Hattiesburg, USA), and were stored at room temperature. β-D Galactose Pentaacetate (sugar acetate, SA) was supplied from Sigma-Aldrich (Darmstadt, Germany). Molecular structures of used molecules are given in Figure 2.1 and Figure 2.2.

Chloroform (≥99.8% purity) was supplied from Merck (Darmstadt, Germany). Carbon dioxide (99.9% purity) was purchased from Linde Gas (Kocaeli, Turkey). For the drug release studies Ceftriaxone Sodium ($C_{18}H_{16}N_8Na_2O_7S_3 \cdot 3.5H_2O$; Mw=661.60 g/mol, Nobel Kimya, Duzce, Turkey), which is a test model antibiotic, was used. When preparing the phosphate buffered saline (PBS) solution, dipotassium phosphate (K_2HPO_4, Mw=174.2 g/mol, ≥97.5% purity) (BDH Chemicals, Poole, England), monopotassium phosphate (KH_2PO_4, Mw=136.1 g/mol, ≥98% purity) (Riedel-de Haën, Seelze, Germany), potassium hydroxide (KOH, Mw=56.11 g/mol, ≥84% purity) (Merck, Darmstadt, Germany), sodium chloride (NaCl, Mw=58.44 g/mol, ≥99.5% purity) (Carlo Erba Reagenti, Cornaredo, Italy), and distilled water (solution medium) were used.

3.2. Polymer Film Preparation

P_LLA films were produced by using solvent casting method. The polymer solution was prepared by dissolution of the weighted amount of polymer in chloroform (the ratio of $CHCl_3$/P_LLA is 8 mL chloroform/g polymer). For the composite films prepared with SA addition, SA was added to the solution as 30 wt % of the resulting P_LLA-SA composite and they were prepared by using 0.5 grams of polymer. For the composite films prepared with POSS addition, one of the POSS (either IPOSS or MPOSS) was added to the solution as 10 wt % of resulting P_LLA-POSS composite and they were prepared by using 0.6 grams of polymer. The solution was mixed with the magnetic stirrer for 3 to 4 hours in a sealed glass bottle to prevent solvent evaporation. SA and both liquid POSS types were soluble in chloroform which resulted in a homogeneous solution. The total solution having polymer-additive-chloroform was poured on a glass plate that has dimensions of 2.5 cm×7.6 cm and kept at room temperature for about 2 hours to evaporate the solvent. After drying to some extent, a second glass plate was placed onto the polymeric film to avoid bending of the film and it let drying for overnight at ambient conditions. The system was then placed in a vacuum oven and drying was continued under vacuum for at least 13 hours. The produced films were stored in a desiccator. Samples (2 cm×3 cm) which were used for $scCO_2$ processing were prepared from the dried films by cutting them. Polymer films prepared with MPOSS and IPOSS were expressed as MP$_L$LA and IP$_L$LA, respectively and their thicknesses were measured as 350±40 μm.

3.3. Processing of Polymers with $scCO_2$

$scCO_2$ processing of the films was performed in a well-sealed stainless-steel high-pressure vessel (Micro Reactor model 4592, Parr Instruments, USA) (Figure 3.1) with a heating jacket. The vessel was coupled with a thermocouple (OMEGA, KMQXL-IM150U-150 OR K type), pressure transducer and a reactor controller (Model 4848, Parr Instruments, USA) to monitor the pressure and control the temperature of the

vessel. Pressurized CO_2 was introduced to the vessel by means of a syringe pump (Model 260D, Teledyne ISCO, USA).

Teflon sheets were placed in the vessel as a barrier between the sample and the vessel wall. The film sample was placed in the vessel, the vessel was sealed and heated to the saturation temperature (ST=313 K). The vessel was then pressurized to the desired saturation pressure (SP=10.3 MPa or 20.7 MPa) with $scCO_2$. At the end of the saturation time (S_{time}=2 h or 24 h), the system was depressurized with a specific venting rate (VR=0.4 MPa/min or 10.9 MPa/min). The processed sample was taken out of the vessel immediately after the depressurization process and let cool at the ambient conditions.

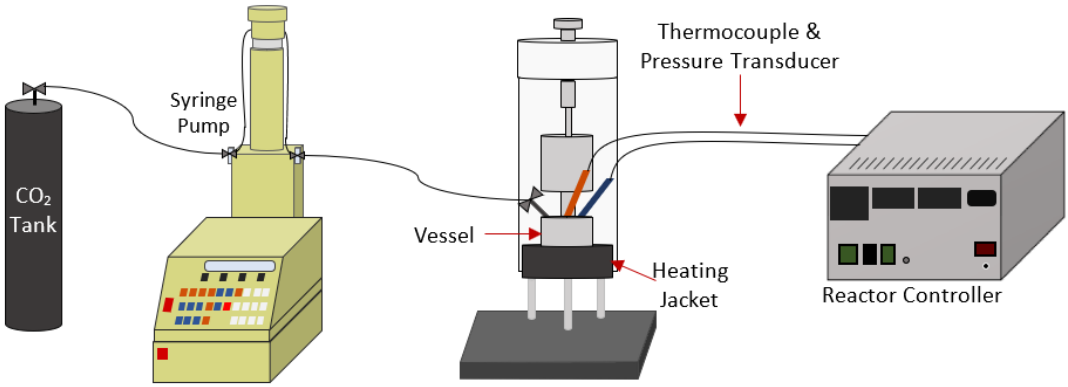

Figure 3.1. Experimental set-up

3.4. Surface Modification with Plasma Etching

The samples which were used in drug release studies were treated with oxygen plasma to enhance the hydrophilicity of the polymer surfaces. Therefore, low-temperature oxygen plasma (Femto 40 kHz, Diener Electronic, Germany) was applied to both sides of the films for 15 minutes at 50 Pa vacuum with 50W power.

3.5. Characterization of The Films

3.5.1. Thermal Properties

The thermal properties of the samples were analyzed with Differential Scanning Calorimetry (DSC) (Model DSC 8000, Perkin Elmer, United States) before and after the $scCO_2$ processing. DSC analysis was carried out under nitrogen environment with the heating rate of 10 K/min and in the temperature range of 263-473 K. The glass transition temperature (T_g) and the specific melting enthalpy (ΔH_m) of the samples were obtained from the first heating thermogram. The degree of crystallinity (X_{Crys}) of the samples were calculated by using Equation 3.1 [75];

$$X_{Crys} = \frac{\Delta H_m + \Delta H_c}{\Delta H_m^o (w_{P_LLA})} \quad (3.1)$$

where ΔH_c is the cold crystallization enthalpy of the sample obtained from the DSC analysis. ΔH_m and ΔH_m^o are the melting enthalpies of semi-crystalline and 100 % crystalline P_LLA (given as 93.1 J/g in the literature [76]), respectively. w_{P_LLA} is the weight fraction of the P_LLA in the analyzed sample. w_{P_LLA} value is taken as 90 % for the unprocessed films and 100 % for the processed films since almost all the added POSS removed from the matrix after $scCO_2$ processing.

3.5.2. Morphological Properties

Morphology of the porous films were determined by scanning electron microscopy (SEM) (Quanta 400 FEG, FEI, USA). The cross-sections of the samples were analyzed after freeze fracture was applied in liquid nitrogen. The samples were coated with Au-Pd and SEM micrographs were obtained with application of 10 kV to prevent charge accumulation. To determine the average pore sizes of the samples, at least 600 pores were randomly selected from the micrographs of one sample and their sizes were measured using Image J software (National Institutes of Health, USA). The average pore diameter was calculated using Equation 3.2;

$$d_a = \frac{\sum d_i \cdot n_i}{\sum n_i} \quad (3.2)$$

where d_a is the average pore diameter, d_i is the pore diameter of a single pore and n_i is the number of pores that were measured. Pore density of the samples was calculated by the same software. The ratio of the porous area to the total area was calculated from randomly selected 3 different areas for each sample. Energy-dispersive X-ray spectroscopy (EDX) analyses and mapping of the samples were carried out to detect the presence or distribution of the POSS (additive) and/or chloroform (solvent) in the samples. The SEM images of all samples processed at all the conditions were obtained and the ones given in the thesis were applied in the Design of Experiments (DoE). The images of the samples which are not included in the Results and Discussion are given in Appendix A.

3.5.3. Mechanical Properties

Tensile instrument (Zwick-Roel, Z250, USA) was used to determine the mechanical properties of the films. Prior to the analyses, the samples were dried at vacuum at least 13 hours. The dried films were tested with a crosshead speed of 5 mm/min. The gauge length and the width of the samples were 20 mm and 4 mm, respectively. Tests were performed for 3 times for each sample and average values of elastic modulus and % elongation at break were determined.

3.6. Drug Release Studies

In drug release studies, PBS solution (0.01 M, pH=7.4) was used as drug release and drug loading medium. Ceftriaxone Sodium was used as a model antibiotic which is soluble in PBS. Prepared Ceftriaxone Sodium-PBS solution (1 g/L) was loaded in the oxygen plasma-treated films (0.5 cm×0.5 cm) via vacuum-pressure cycle. For this purpose, films were placed in a desiccator and 5 µL of drug solution was dropped on each film. Next, the vacuum was applied for 10 minutes and then was released to push the drug-containing solution into the porous matrix. This cycle was repeated for four

times for each drop of drug solution. Overall, 50 μL of drug solution (50 μg drug) was loaded to the films equally from both sides. Drug release analysis was performed by immersing the drug-loaded films in 3 mL of PBS solution at around the human body temperature (310±1 K). PBS solutions were replaced with fresh ones at various time intervals and the taken media was analyzed with UV–vis spectrophotometer (8453 UV–vis, Agilent Technologies, USA) to detect the amount of the released drug. Maximum wavelength of the absorption of the drug was found as 241 nm in PBS solution. The calibration curve was obtained by using drug solutions prepared at various concentrations. Three replicate experiments were carried out for each sample.

CHAPTER 4

RESULTS AND DISCUSSION

4.1. Sugar Acetate (SA) Foaming Experiments

There are different studies focused on the SA-CO_2 binary systems in the literature. In one of them, which was a phase equilibrium study, Potluri *et al.* stated that SA is well dissolved in supercritical carbon dioxide, and observed the formation of a fragile SA foam when they removed CO_2 from the system [70]. However, this was only an observation without a structural characterization being carried out. Zhang *et al.* obtained fibrillated brittle SA foam when they froze the SA-CO_2 binary system in liquid nitrogen in a directional way and using a different approach from Potluri *et al.*, they sublimed CO_2 instead of fast venting [77].

In the light of this information, foaming of the two-phase SA-CO_2 system was studied firstly. To do that, SA was liquefied in the pressurized SA-CO_2 system, and the pressure was set to 12.6 MPa at 323 K. After equilibrium was achieved, the system was rapidly depressurized. SEM images of the obtained samples are given in Figure 4.1. There are some pores in the scCO_2-processed SA samples distributed heterogeneously and they are not uniform. These pores might have formed with the separation of CO_2 from the liquefied SA, forming bubbles which stabilized as the SA solidified with decreasing pressure.

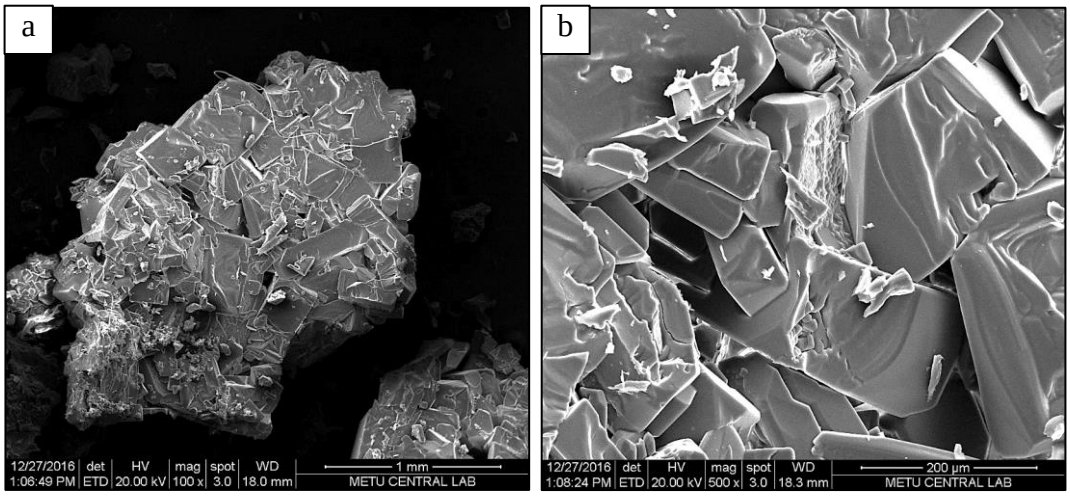

Figure 4.1. SEM images of SA samples after foaming at 12.6 MPa at 323 K with (a) 100x magnification (scale bar=1 mm) (b) 500x magnification (scale bar=200 µm)

Single phase SA-CO_2 system was studied later at 323 K and 17.2 MPa. After the equilibrium condition was achieved, CO_2 was removed from the system by venting. SEM images of the obtained samples are given in Figure 4.2. According to these images, in addition to pores, different crystalline structures were observed. Observed pores are distributed heterogeneously in the sample, and they are regionally located. The crystalline sample was obtained after depressurizing SA-CO_2 single phase system.

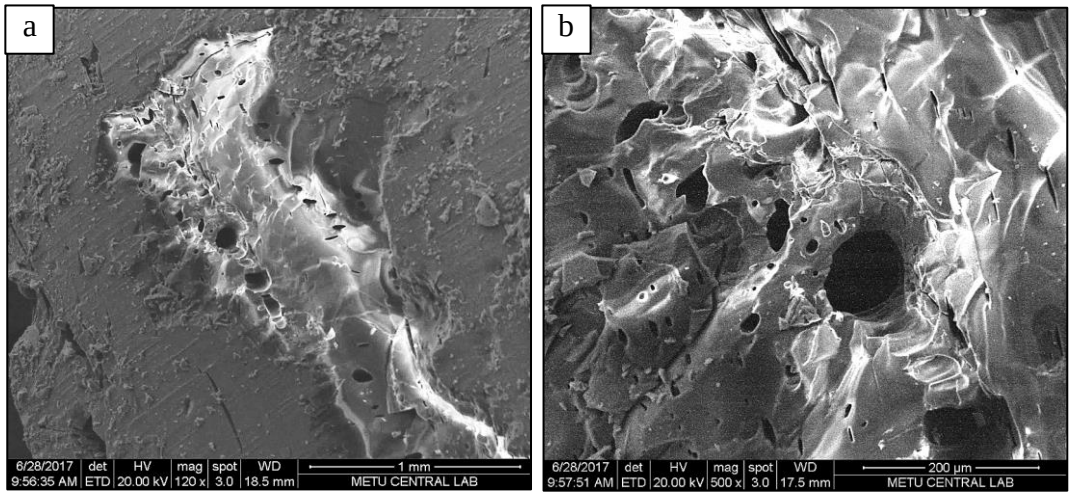

Figure 4.2. SEM images of samples of SA foaming experiment at 17.2 MPa at 323 K with (a) 120x magnification (scale bar=1 mm) (b) 500x magnification (scale bar=200 µm)

Potluri *et al*. stated in their solubility study of SA in CO_2 that they observed a fragile foam structure of SA without any structural analysis. SA samples that we obtained after the $scCO_2$ foaming were also fragile. On the other hand, even if the structure of SA looked like foam, the SEM images showed that its microstructure was not actually porous and so it was concluded that there was no proper pore formation in the sample. Therefore, the experiments related to the foaming of SA in $scCO_2$ were not carried further.

4.2. P_LLA Foaming Experiments

4.2.1. Porous Pellet Preparation with $scCO_2$ Processing

At the beginning of this thesis study, pellet type of samples were studied in foaming experiments instead of film type to increase the application area of the polymer.

4.2.1.1. $scCO_2$ Processing of Neat P_LLA Pellets

In an earlier study conducted in our laboratory, Novendra *et al*. obtained polymer matrices via solvent casting which resulted in thin films with a thickness of 250±50

μm [38]. In this study, as a continuation of the previous study, a new sample preparation method was applied to obtain thicker samples. The aim to enhance the mechanical properties of the matrices, and therefore to widen their application area.

Polymer pellets were prepared by using 200 mg P_LLA powder (particle size<300 nm) was obtained with cryogenic grinding of granular P_LLA, and by compressing the powder with 20 MPa pressure for 10 minutes. Weights of the pellets were measured as 195±5 mg and their diameters and thicknesses were 12.25 mm and 1.48±0.02 mm, respectively. SEM images of the unprocessed neat P_LLA are given in Figure 4.3(a). Since there is no binder (like chloroform for sticking the particles to increase rigidity) in the pellets, small cracks and hallows were observed in their cross-sections. Also, the pellets were very brittle. To observe the sole effect of $scCO_2$ processing on neat P_LLA pellet, it was processed with $scCO_2$ at 313 K and 20.7 MPa for 24 hours with a depressurization rate of 10.9 MPa/min. These mentioned conditions were chosen because, in the previous studies, it was observed that the most efficient foaming was obtained under these conditions. In this previous study a highly crystalline P_LLA-POSS film in which a fluorinated and solid CO_2-philic POSS was used as a cell nucleating agent and processed with $scCO_2$ [38]. SEM images of the processed sample are given in Figure 4.3(b). According to the SEM images, there is no pore formation after the $scCO_2$ processing of the pellets. This result is similar to the previous study which indicates that semi-crystalline P_LLA samples cannot be foamed at low temperatures and pressures without using CO_2-philic pore inducers even if different sample preparation methods were applied. On the other hand, $scCO_2$ penetrated into the pellets with the help of the early mentioned cracks and hallows and made them larger, while the pellets were still very brittle.

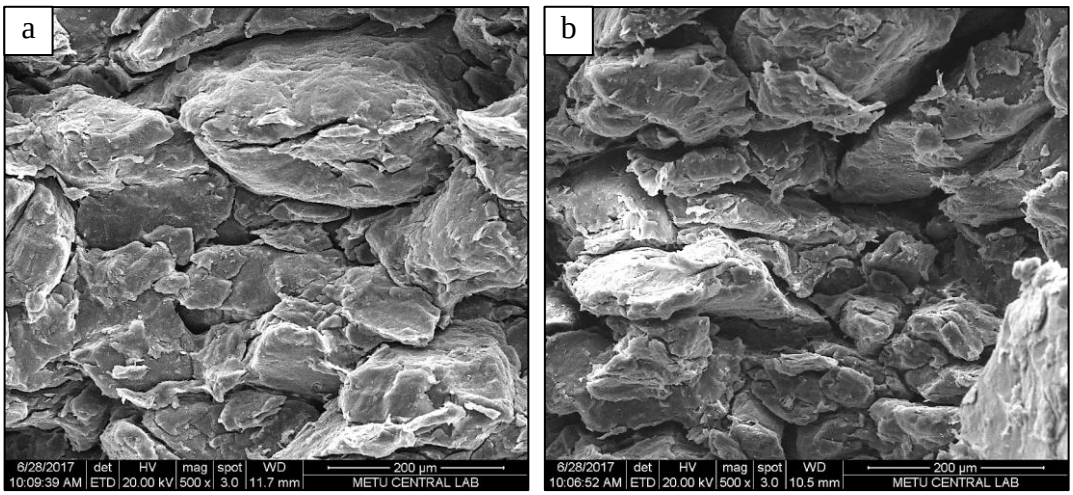

Figure 4.3. SEM images of the neat P_LLA pellets (a) unprocessed and (b) $scCO_2$ processed at 313 K and 20.7 MPa for 24 hours with a depressurization rate of 10.9 MPa/min (scale bar =200 μm for both images)

4.2.1.2. $scCO_2$ Processing of P_LLA Pellets Prepared with Additives

Novendra *et al*. were able to foam semi-crystalline P_LLA at low temperature and pressure by using CO_2-philic pore inducer, trifluoropropyl POSS (TFPOSS) [38]. In this study, SA was used instead of TFPOSS because of its more labile molecular structure and bio-compatible nature. Therefore, pellets were prepared by using a powder mixture of P_LLA-SA (with 30 wt. % SA) and chloroform was added to powder and obtain paste-like mixture to make more rigid structure. A paste-like mixture was aimed to keep the integrity of the sample after $scCO_2$ processing, and to produce pellets with a homogeneous structure. Therefore, 120 μL of chloroform was mixed with 210 mg of P_LLA-SA powder mixture gradually. The paste-like mixture was placed on the vessel of the pellet making machine immediately to prevent evaporation of chloroform and keep the paste form. The mixture was pressed under vacuum by applying 20 MPa pressure for half an hour. The pellet sample was kept in the vacuum oven for 13 hours at ambient conditions to remove the remaining chloroform. Then, the sample was processed with $scCO_2$ at 313 K and 20.7 MPa for 24 hours with a depressurization rate of 10.9 MPa/min. SEM images of the processed sample are given

in Figure 4.4. The cross-section of the pellet was more homogeneous than the former one, but the pore distribution was not homogeneous. Pellet kept its integrity after $scCO_2$ foaming.

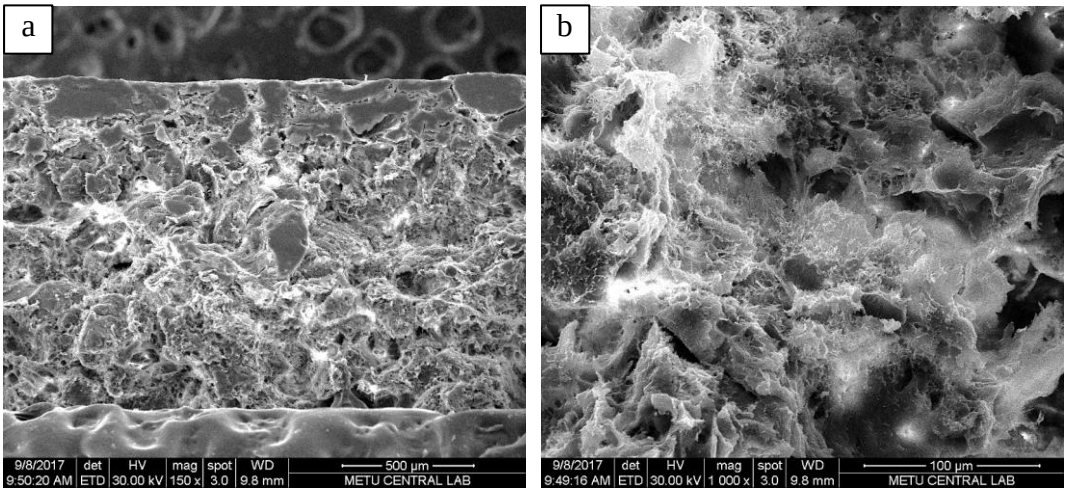

Figure 4.4. SEM images of the cross-section of $scCO_2$ processed P_LLA-SA pellets at 313 K and 20.7 MPa for 24 hours with depressurization rate of 10.9 MPa/min with (a) 150x magnification (scale bar=500 µm) (b) 1000x magnification (scale bar=100 µm)
(wetted with 120 µL chloroform and dried in a vacuum oven for at least 9 hours at 383 K)

In order to observe the distribution of the additive in the pellet prepared with the last-mentioned technique, EDX analysis was carried out. For this purpose, another additive containing different atoms than P_LLA was used to observe the additive distribution by the EDX analysis. This additive should be also soluble in CO_2 to induce pore formation during $scCO_2$ processing. Therefore, octatrimethylsiloxy POSS (SPOSS), which has Si atoms was used as a pore inducing agent at 30 % by weight. In order to observe whether this technique is reproducible, three separate pellets were prepared under the same condition. One of them was processed with $scCO_2$ and the foaming properties were studied, whereas the others were analyzed with SEM and the reproducibility of the technique was compared. All samples were kept in the vacuum oven for 13 hours at ambient conditions. SEM images of two replicates of unprocessed

samples are given in Figure 4.5. According to EDX results, SPOSS agglomerate throughout the cross-section in both samples and even if they were prepared with the same method, their structures were not similar and not homogeneous. Therefore, it was decided that the pellet making method is not reproducible for $scCO_2$ processing of P_LLA samples.

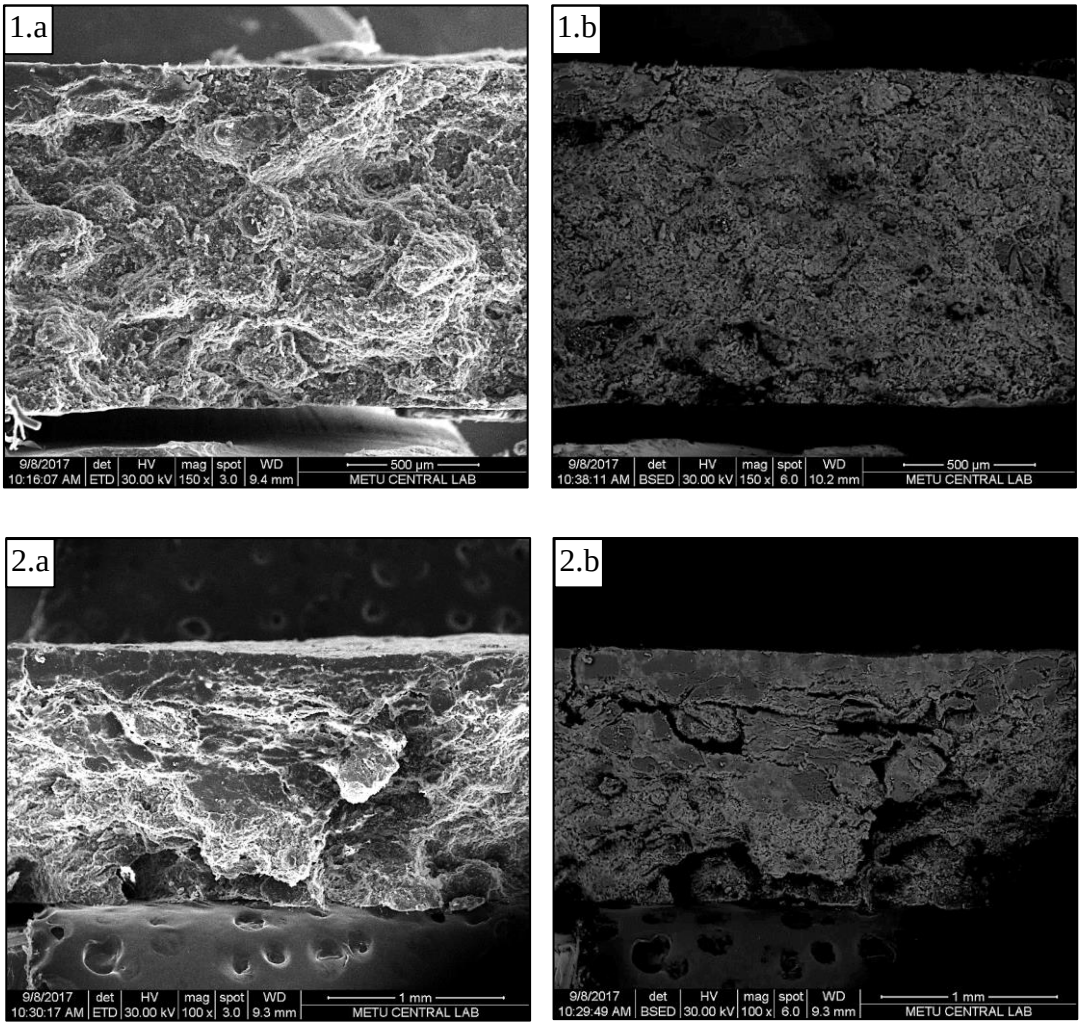

Figure 4.5. SEM images of the cross-section of (a) P_LLA-SPOSS, b) SPOSS distribution in the same unprocessed pellet
(scale bar=500 µm for 1(a) and 1(b); scale bar=1 mm for 2(a) and 2(b))

The other pellet was processed with $scCO_2$ at 313 K and 20.7 MPa for 24 hours with a depressurization rate of 10.9 MPa/min. Its SEM image is given in Figure 4.6. It can be seen that; the pore distribution was more homogeneous than those of the processed P_LLA-SA pellets (wetted with chloroform after preparing). Also, pellet kept its structural integrity. Since this technique is not reproducible, no further analysis was performed on the pellets. In the following studies, solvent cast films were studied.

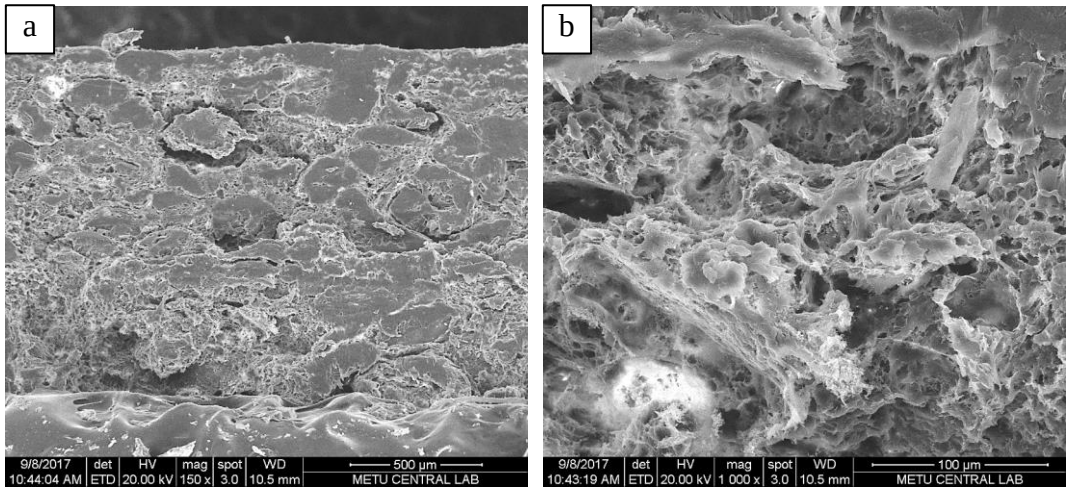

Figure 4.6. SEM images of the cross-section of the $scCO_2$ processed P_LLA-SPOSS pellet at 313 K and 20.7 MPa for 24 hours with a depressurization rate of 10.9 MPa/min with different magnifications(a) 150x magnification (scale bar=500 µm) (b) 1000x magnification (scale bar=100 µm)

4.2.2. Porous Film Preparation with $scCO_2$ Processing

4.2.2.1. $scCO_2$ Processing of Neat P_LLA Films

In order to obtain homogenous structures and reproducible samples, solvent casting method was used in this study from now on. Therefore, neat P_LLA films were cast and processed with $scCO_2$ (before the composite films) to observe the sole effect of $scCO_2$ on polymer. Therefore, solvent cast P_LLA film was prepared with 0.5 grams of the polymer by the method mentioned in Section 3.2. The SEM image of the neat P_LLA

film is given in Figure 4.7(a). Solvent cast film has a homogeneous structure, unlike pellets. The film was also processed with $scCO_2$ at 313 K and 20.7 MPa for 24 hours with a depressurization rate of 10.9 MPa/min and its SEM image is given in Figure 4.7(b). As it can be seen from the image, there is no pore formation after $scCO_2$ processing which is an expected result since Novendra *et al.* observed similar results and no pore formation in the neat P_LLA films processed under the same conditions without pore inducers [38]. It was observed that the neat P_LLA films were highly flexible before and after the $scCO_2$ processing.

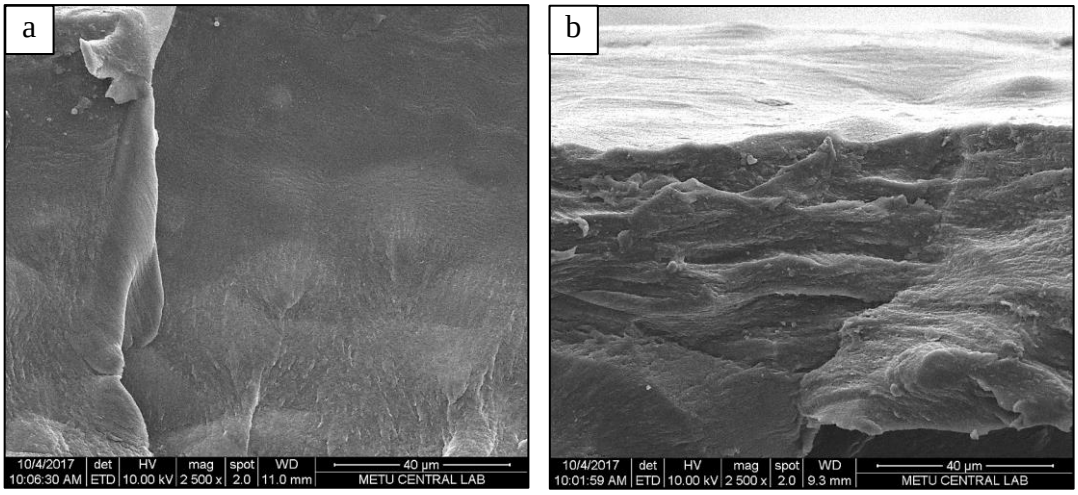

Figure 4.7. SEM images of the neat P_LLA film (a) unprocessed and (b) $scCO_2$ processed at 313 K and 20.7 MPa for 24 hours with a depressurization rate of 10.9 MPa/min
(scale bar=40 µm for both images)

4.2.2.2. $scCO_2$ Processing of Composite P_LLA Films

In order to increase the affinity of the polymer matrix for CO_2, CO_2-philic additives were introduced into the matrix during the solvent casting procedure. Similar to the pellets and earlier study conducted in our laboratory by Novendra *et al.*, it was expected that the additives act as pore inducers and $scCO_2$ processing results in a porous matrix. Therefore SA, IPOSS and MPOSS which are CO_2-philic were used.

4.2.2.2.1 $scCO_2$ Processing of P_LLA-SA Films

SA was used as an additive in polymer matrix since it has benign nature and high solubility in CO_2. Therefore, in the solvent casting process, SA was added into the mixture by 30 wt % and the mixture was stirred to complete dissolution of the solids. The crystalline structure of the SA made composite polymer-SA film brittle. Obtained films were processed with $scCO_2$ at 313 K and 20.7 MPa for 24 hours with a depressurization rate of 10.9 MPa/min. The SEM images of the unprocessed and processed films are given in Figure 4.8. After processing, the film retained its fragility. As can be seen from the SEM images, SA acted as a good pore-nucleating agent. The submicron-sized pores are homogeneously distributed throughout the sample. However, the lack of ductility of the film may cause problems in the application stage. Therefore, studies with P_LLA-SA films were ended at this stage.

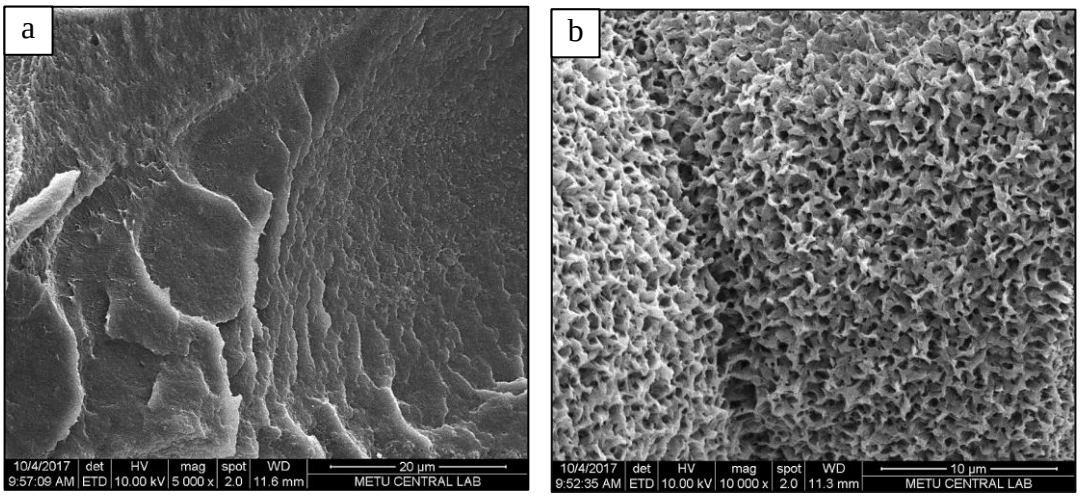

Figure 4.8. SEM images of the P_LLA-SA film (a) unprocessed (scale bar=20 μm) and (b) $scCO_2$ processed at 313 K and 20.7 MPa for 24 hours with a depressurization rate of 10.9 MPa/min (scale bar=10 μm)

4.2.2.2.2 $scCO_2$ Processing of P_LLA- Liquid POSS films

Since the solid additives used in the polymer matrix in this study (SA) and in the previous study conducted in our laboratory by Novendra *et al*. (TFPOSS), resulted in brittle polymer films, it was decided to use biocompatible and CO_2-philic liquid POSS (isooctyl POSS (IPOSS) and methacrylisooctyl POSS (MPOSS)) as pore inducers. Due to the multiple numbers of process parameters, a DoE was applied to P_LLA-liquid POSS films in the foaming experiments.

4.2.3. Porous Film Preparation with P_LLA-Liquid POSS Composites by Using DoE

The neat P_LLA films obtained by solvent casting were homogenous similar to the previous one. The thicknesses of the neat P_LLA film and P_LLA-POSS composite films were about 350±40 μm. The T_g and T_m of the control P_LLA films, which were neat and unprocessed, were found as 308 and 454 K, respectively with DSC analysis. (DSC thermograms are given in Appendix B). The low T_g value of the neat P_LLA can be attributed to remaining chloroform in the samples which acts as a plasticizer that decreases the intermolecular forces and increases the chain mobility [78], which was extracted from the polymer almost completely during the supercritical CO_2 processing (Elemental EDX analyses are given in Appendix C). The crystallinity of the control films was calculated as 46 %. Before investigating the effect of CO_2-philic nucleating agent and process conditions on foaming efficiency and foam morphology, neat P_LLA films were processed with $scCO_2$ at 20.7 MPa and 313 K for 24 hours with depressurization rate of 10.9 MPa/min. This particular condition was chosen because it gives the best results in our previous study as mentioned before [38]. This allowed us to observe the sole effect of CO_2 processing on the neat P_LLA films. Similar to the previous study, if there is no nucleating agent, a porous structure was not observed in the SEM images of the cross-section of the sample after the $scCO_2$ processing as seen in Figure 4.9. The inefficiency of $scCO_2$ to foam P_LLA can be attributed to the highly

ordered crystalline structure and thus stiffness of P_LLA, preventing the efficient dissolution of CO_2 in the polymer matrix and thus its plasticization [38,46].

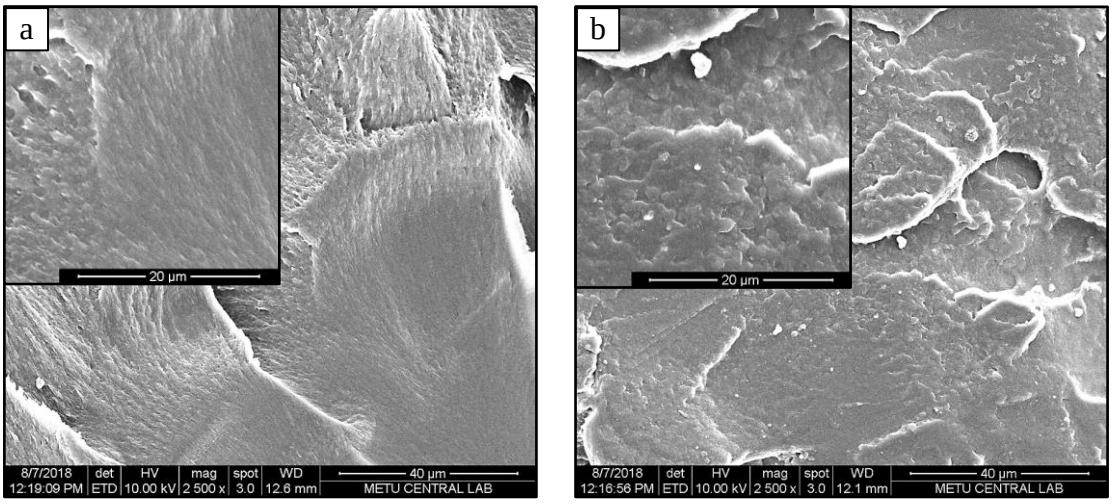

Figure 4.9. SEM images of the cross-section of neat P_LLA films (a) unprocessed and (b) $scCO_2$ processed at SP=20.7 MPa and ST=313 K for S_{time}=24 hours VR=10.9 MPa/min (scale bar=40 µm; inset=20 µm for both images)

In order to increase the affinity of P_LLA matrix to CO_2, and also create nucleation sites in the matrix, two different CO_2-soluble, liquid additives, IPOSS [69] and MPOSS [74] were added to the polymer matrix at 10 wt %, which was the highest additive concentration yielding polymer films without phase segregation. We observed that concentrations higher than this value led to phase segregation and caused a problem in film integrity. In contrast to the solid fluorinated POSS cell nucleator, the addition of liquid IPOSS or MPOSS into the P_LLA matrix resulted in a porous structure in the films obtained with solvent casting, even prior to the $scCO_2$ processing, as seen in Figure 4.10. The POSS molecules acted as pore nucleating agents in the solvent casting procedure. The homogenous pore distribution was observed probably as a result of the well-distribution of the POSS molecules in the composite matrix, verified by the EDX mapping analysis of the entire cross-section of the films which is shown

in Figure 4.11. The homogenous dispersion of cell nucleating agents is advantageous since it enhances the $scCO_2$ foaming performance of the nucleating agent in the matrix during the foaming process [6]. Besides their enhancing contribution on the foaming of P_LLA, CO_2-philicity of the additives also allowed extraction of almost all of the additives by the supercritical fluid. The extraction of POSS was verified with the EDX analyses of the $scCO_2$-processed thin films (Elemental EDX analyses are given in the Appendix C). This provides an additional advantage in the process regarding the recovery of the expensive cell nucleating agents and production of almost pure porous films free of additives, making them preferable for drug delivery applications without affecting the biodegradability of the polymer. The $scCO_2$-processed porous P_LLA obtained with the liquid IPOSS or MPOSS used as the CO_2-philic cell nucleator was not fragile and rigid as the one obtained with the solid fluorinated POSS cell nucleator [38] and exhibited a ductile nature.

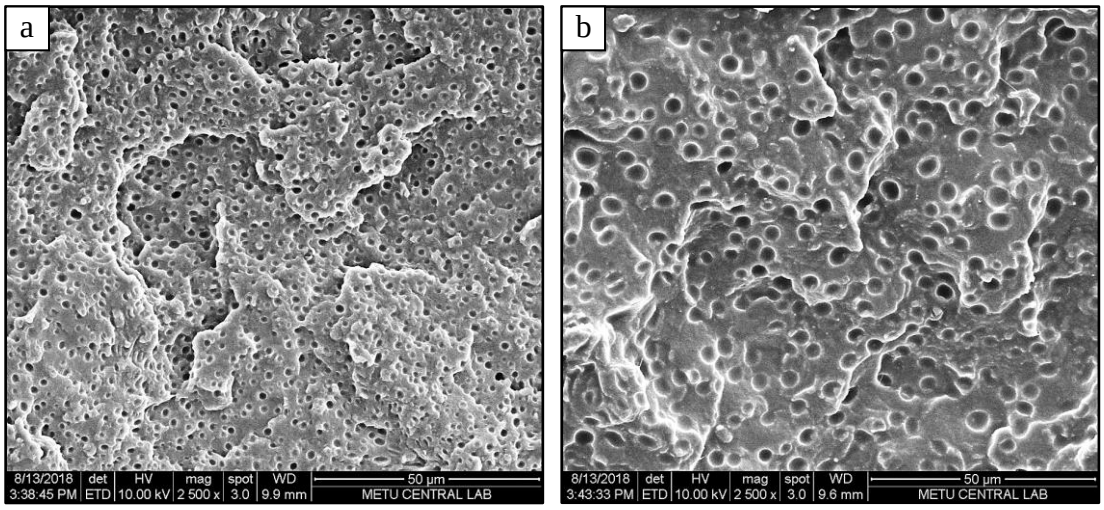

Figure 4.10. SEM images of the cross-section of the unprocessed (a) MP_LLA and (b) IP_LLA films (scale bar=50 µm for both images)

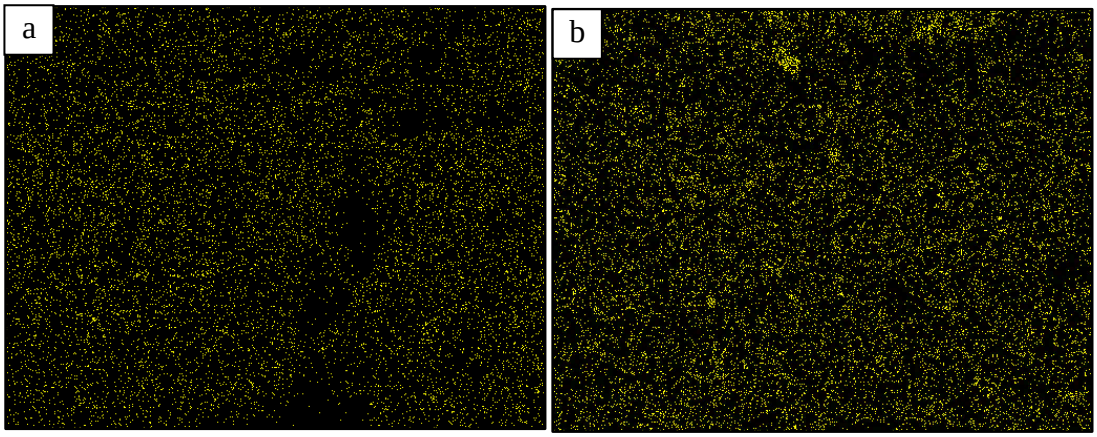

Figure 4.11. EDX mapping (silicone map) of the cross-section of the entire thickness of unprocessed (a) MP_LLA and (b) IP_LLA films (with 1000x magnification)

For systematic determination of the effect of the process conditions on the pore morphology and foaming efficiency, design of experiment (DoE) was applied, using the two-level full factorial method. The design parameters are given in the Table 4.1. Keeping the process temperature constant at 313 K, different saturation pressure, saturation time and venting rate were applied. The labeling of the processed samples were denoted as MP_LLA-SP-S_{time}-VR, where SP is the saturation pressure, S_{time} is the saturation time and VR is the venting rate (as slow (s) or fast (f), respectively).

Table 4.1. *Process parameters applied in DoE*

Process Parameters	Low Value	High Value	Unit
Saturation Pressure (SP)	10.3	20.7	MPa
Saturation Time (S_{time})	2	24	Hour
Venting Rate (VR)	0.4	10.9	MPa/min

4.2.3.1. Pore Morphology of the Films

In order to evaluate the effect of $scCO_2$ processing parameters on the foaming efficiency and pore morphology, the average pore diameter and pore density were

calculated for all the unprocessed and processed composite films, which are given in Figure 4.12. The average pore diameter of the unprocessed MP_LLA film was measured as 1.4±0.3 μm. Both, $scCO_2$ processing and process conditions did not affect the average pore diameter of the MP_LLA films significantly, and the average pore diameter of the all processed films was about 1.6±0.5 μm. Meanwhile, the average pore size of the unprocessed IP_LLA film was calculated as 3.3±0.6 μm. When these films were processed at the lower pressure for 24 hours, the size of the pores increased by about 1.6 times and the average pore diameters were obtained as 5.2±1.2 μm with both fast and slow venting rates. The shorter processing time decreased the average pore diameter of the films to 2.2±0.5 μm, which was independent of the pressure and venting rate. Generally, independent of the processing conditions, all the IP_LLA films had a larger average pore diameter than their counterparts with MPOSS. This is probably due to different affinities of these POSS types to the polymer and CO_2, affecting not only their agglomeration size in the polymer film formed with solvent casting but also their dissolution kinetics into carbon dioxide during the supercritical batch foaming and coalescence of the nucleating bubbles during the depressurization.

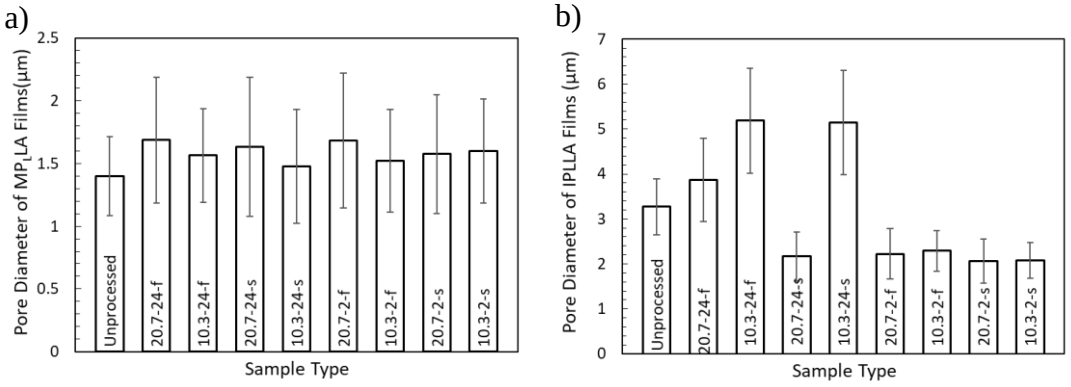

Figure 4.12. Pore diameters of the (a) MP_LLA (b) IP_LLA films (Labeling of the processed samples were denoted as SP-S_{time}-VR, where SP is the saturation pressure (10.3 or 20.7 MPa), S_{time} is the saturation time (2 or 24 hours) and VR is the venting rate (0.4 or 10.9 MPa/min as slow (s) or fast (f), respectively))

Pore densities of all the unprocessed and processed films are given in Figure 4.13. For all the processed films at constant saturation time and venting rate, the pore density decreased with decreasing saturation pressure, which can be attributed to the decreasing CO_2 solubility in the polymer matrix. The pore densities of unprocessed MP_LLA and IP_LLA films were almost similar, as 19.2±1.6 % and 20.8±0.4 %, respectively. Among all the films, the highest pore density was obtained in those processed at 20.7 MPa for 24 hours and depressurized with the venting rate of 10.9 MPa/min. This was valid for both and MP_LLA and IP_LLA films and found as 29.4±2.4% and 28.5±2.4%, respectively. The close pore densities of the processed films with MPOSS and IPOSS can be attributed to the similar solubility of these molecules in $scCO_2$, which indicate a similar level of CO_2-philicity [69,74]; for example, at 308 K, the solubility of IPOSS in $scCO_2$ is 3.6×10-4 at 14.3 MPa, while that of MPOSS is about 4.1×10-4 at 12.6 MPa. The SEM images of these processed films are given in Figure 4.14, which is also a representative image of all the processed films, exhibiting homogeneous pore distributions and closed-cell structure (SEM images of the films processed at different conditions are given in Appendix A.). This obtained closed pore structure after $scCO_2$-processing may result from restricted pore nucleation and growth at low temperatures [54]. CO_2 diffusivity in the polymer matrix will be limited if viscosity and modulus of the polymer are not low enough which restricts the pore nucleation and growth in the matrix and resulting in the closed pore structure. While the pore density of the supercritical CO_2-processed film (Figure 4.14) was greater than the unprocessed film (Figure 4.10), the pore morphologies of both films were similar. The pores formed during both solvent casting and supercritical fluid processing only when the polymers were composites of P_LLA and POSS. No pore formation was observed when neat P_LLA film was cast with chloroform or processed with supercritical CO_2. This shows that POSS acted as a cell nucleator in both processes, and therefore the morphologies of both porous polymers were similar.

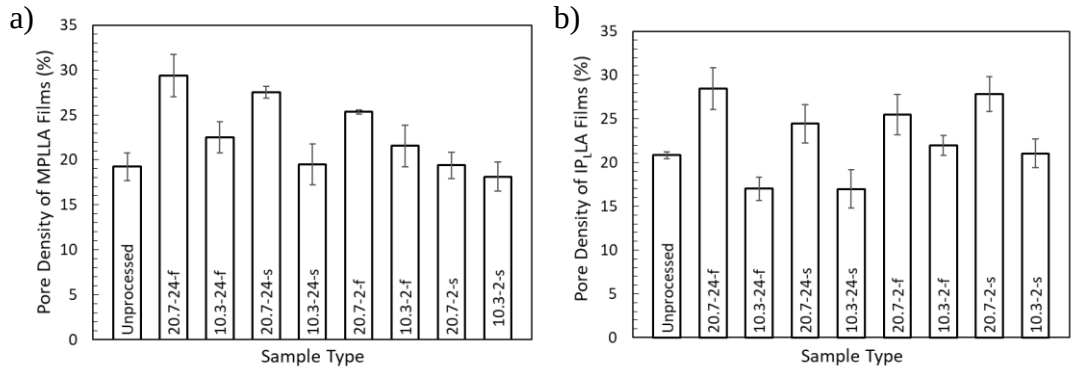

Figure 4.13. Pore density of the (a) MP_LLA (b) IP_LLA films (Labeling of the processed samples were denoted as SP-S_{time}-VR, where SP is the saturation pressure (10.3 or 20.7 MPa), S_{time} is the saturation time (2 or 24 hours) and VR is the venting rate (0.4 or 10.9 MPa/min as slow (s) or fast (f), respectively))

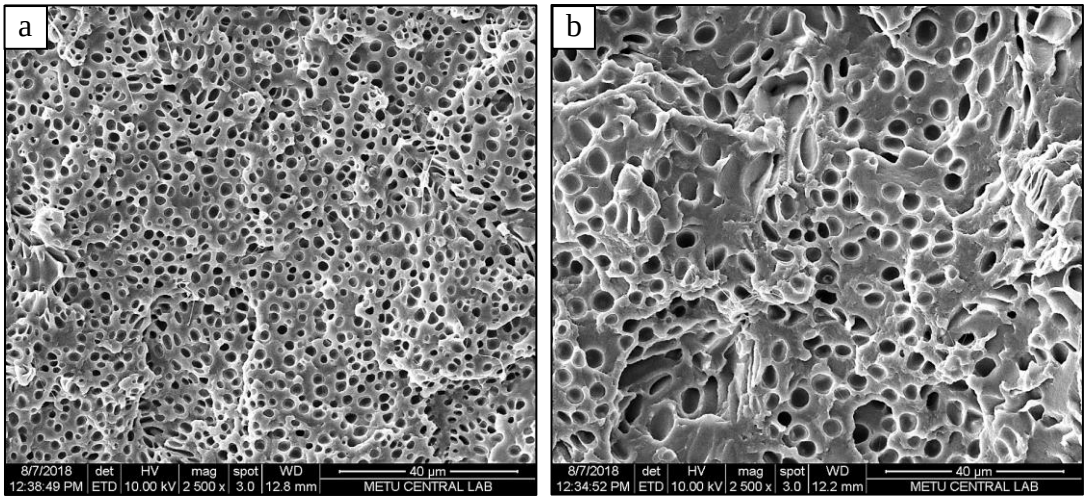

Figure 4.14. SEM images of the cross-section of $scCO_2$ processed at SP=20.7 MPa and ST=313 K for S_{time}=24 hours VR=10.94 MPa/min (a) MP_LLA and (b) IP_LLA films (scale bar=40 µm for both images)

4.2.3.2. Thermal Analysis of Film (DSC)

DSC analyses were performed on all the unprocessed and processed films to observe the effects of the CO_2-philic additive and $scCO_2$ processing conditions on thermal properties and crystallinity of the porous films. The results of the analyses are given in Table 4.2 and Table 4.3 for MP_LLA and IP_LLA, respectively. DSC graphs of all samples are given in Appendix B. According to the DSC data, the glass transition temperature (T_g) of the neat polymer, which was 308 K, increased with the addition of MPOSS and IPOSS to 312 K and 315 K, respectively, which is in agreement with the literature, and also states that the presence of the POSS molecules in the P_LLA polymer matrix improved its thermal features like T_g [56]. Further increase in T_g was observed in all the $scCO_2$-processed films with both types of CO_2-philic cell nucleators, indicating local chain ordering and enhanced intermolecular interactions in the amorphous matrix of the polymer. This is thought to occur during the $scCO_2$-processing with CO_2 dissolving in the polymer, leading to increased chain relaxation, mobility and free volume, which results in the local realignment of the chains in the amorphous region [46]. Another reason of the increase in the T_g of the processed polymers is believed to be the removal of the chloroform residue extracted by supercritical CO_2 during the batch foaming, which further improved the T_g (as shown in the EDX analyses in the Appendix C). Independent of the processing parameters or the POSS type, T_g of all the processed composite films were similar, with an average T_g of 330±2 K. On the other hand, melting temperature of the samples showed almost no change with addition of POSS molecules and application of foaming process, and it was 455±1 K for all the films. Similarly, the crystallinity of the films was not affected either by the addition of the liquid CO_2-philic POSS nor the $scCO_2$ processing conditions and the average crystallinity of all the films was determined about 47±1 %. This is in contrast to our previous study in which a solid POSS was used in foaming of P_LLA and resulted in increased both T_g and T_m of the polymer [38].

Table 4.2. *DSC results of the MP_LLA composites*

Sample Name	T_g (K)	T_m (K)	Crystallinity (%)
P_LLA	308	454	46
MP_LLA	312	454	45
MP_LLA -20.7-24-f	331	455	47
MP_LLA -10.3-24-f	327	455	46
MP_LLA-20.7-24-s	330	455	49
MP_LLA-10.3-24-s	330	454	47
MP_LLA-20.7-2-f	326	455	49
MP_LLA-10.3-2-f	329	454	46
MP_LLA-20.7-2-s	332	455	46
MP_LLA-10.3-2-s	332	455	45

Table 4.3. *DSC results of the IP_LLA composites*

Sample Name	T_g (K)	T_m(K)	Crystallinity (%)
P_LLA	308	454	46
IP_LLA	315	454	48
IP_LLA-20.7-24-f	329	455	47
IP_LLA-10.3-24-f	331	455	47
IP_LLA-20.7-24-s	330	454	48
IP_LLA-10.3-24-s	329	455	47
IP_LLA-20.7-2-f	325	454	48
IP_LLA-10.3-2-f	330	454	45
IP_LLA-20.7-2-s	333	457	46
IP_LLA-10.3-2-s	332	455	45

4.2.3.3. Mechanical Analysis of Films (Tensile Test)

In order to observe the changes in the mechanical behavior of the samples after incorporation of additives and $scCO_2$ processing, the tensile tests were carried out with the films processed at 20.7 MPa for 24 hours and depressurized with the venting rate of 10.9 MPa/min. These films were selected for the mechanical test since the highest pore density for both additive types were obtained when these processing conditions were applied. The results of the tests are given in Table 4.4. The elastic modulus of the neat P_LLA film, which was 0.43 GPa, increased after the addition of the POSS molecules, which are known to enhance the tensile properties of a polymer [56]. Both additives had a similar contribution to the increasing tensile modulus and moduli of the films increased by about 1.4-fold on average. On the other hand, foaming of the composite films with $scCO_2$ had a superior effect on the elastic modulus. Moduli of the MP_LLA films and IP_LLA films increased by about 2-fold, reaching to 1.14 and 1.16 GPa, respectively. Compared to the neat P_LLA films, the increases were about 2.6 times. Although P_LLA has brittle nature and low % elongation value at break (<10%) [79], elongation value of neat P_LLA was found as 290%. This is due to the remaining chloroform residue in the neat P_LLA film which has a plasticizing effect on the polymer matrix and manifests itself in the unusually lower T_g of the polymer film as explained earlier. Rhim et al. observed the same behavior when they prepared P_LLA films with solvent casting and dried at room temperature [78]. They found 203.4 ± 20.8 % elongation at break of solvent cast films, whereas 3.0 ± 0.1 % elongation was obtained with films prepared with hot-press technique. They linked this higher elongation value of solvent cast films to plasticizing effect of the remaining chloroform in the matrix since plasticizers increase the ductility of the samples with increasing the chain mobility. In their next study, Rhim et al. dried solvent cast films at 333K under vacuum to remove all the residual solvent, and they found the elongation of these P_LLA films as 3% [80]. In another study, film drying at 313 K under vacuum for two days, however, it was not successful to remove the chloroform and

elongation of neat P_LLA was found as 158 % [81]. Heat was also not applied to the prepared films in this study in order to preserve the thermal history of the samples. On the other hand, elongation at break decreased from 290% to 92.0% and 82.7%, respectively when MPOSS and IPOSS were incorporated into the polymer matrix. Fernández *et al*. observed similar behavior when using aminopropylheptaisobutyl POSS and aminopropylheptaisooctyl POSS into P_LLA matrix and concluded that polymer brittleness increased since ductility (elongation at break) decreased with the addition of POSS [82]. After $scCO_2$ processing further decrease was observed in % elongation values and it decreased from 92 to 15 % and from 83 to 12 % for MP_LLA and IP_LLA, respectively. The possible reasons of this decrease in the elongation at break are similar to the increase in the T_g of these polymers. One reason can be given as the plasticizing effect of the dissolved CO_2 in the polymer during the supercritical batch foaming leading to local chain realignment enhancing the intermolecular interactions in the polymer [46]. The other reason can be given as the supercritical CO_2 extraction and removal of the residual chloroform from the polymer film during the batch foaming. Removing the residual chloroform (EDX analyses given in the Appendix C) also eliminated its plasticizing effect in the polymer film, increasing the brittleness of the films [78]. Nevertheless, the porous films of MP_LLA and IP_LLA were more ductile materials than the previously foamed P_LLA films in which solid CO_2-philic TFPOSS were used as cell nucleators [25].

Table 4.4. *Tensile test results*

Sample Name	Modulus (GPa)		% Elongation at Break	
	Average	St. Dev	Average	St. Dev
P_LLA	0.43	0.03	290.00	43.59
MP_LLA	0.54	0.05	92.00	19.67
IP_LLA	0.63	0.04	82.67	23.29
MP_LLA-20.7-24-f	1.14	0.05	15.00	2.00
IP_LLA-20.7-24-f	1.16	0.08	12.33	1.53

4.2.3.4. Drug Release Studies

Drug release studies were carried out with both unprocessed and processed porous films by using a model antibiotic, Ceftriaxone Sodium (CS). The release characteristics of the produced films with different pore diameters and pore densities were studied. Since P_LLA films had highly hydrophobic skin, oxygen plasma was performed to increase the hydrophilicity by introducing polar groups on the film surface [38,83–86]. In Figure 4.15.a, the picture shows the drop of the drug solution on the surface of the $scCO_2$-processed IP_LLA films before the oxygen plasma application, while the Figure 4.15.b shows the drug solution drop on the same film after the oxygen plasma application. As the figure shows, this treatment remarkably improved the contact between the drug solution and the polymer, allowed the solution to cover the film surface, and thus eased the migration of the aqueous drug solution into the matrix of the polymeric films. All films exhibited burst release and on average, 88±2 % of the loaded drug released in the first 30 minutes as seen in Figure 4.16. After the initial burst release, the release of the drug continued from the drug-loaded films for two weeks with a slower rate which decreases to 1.6 μg/h from 176 μg/h in 3 hours and decreased further to 0.042 μg/h. In addition, all the films regardless of their pore diameter and pore density exhibited the same trend in the release studies. Burst release of a high amount of drug can be attributed to the presence of the drug on the pores close to the surface and low interconnectivity of the pores in the matrix. This type of release pattern is suitable for local antibiotic applications since, after the immediate effect on the bacteria, a continuous slow release of the drug inhibits further infection at the treated area. These types of matrices can be used in periodontal as well as cancer treatment applications [21,22].

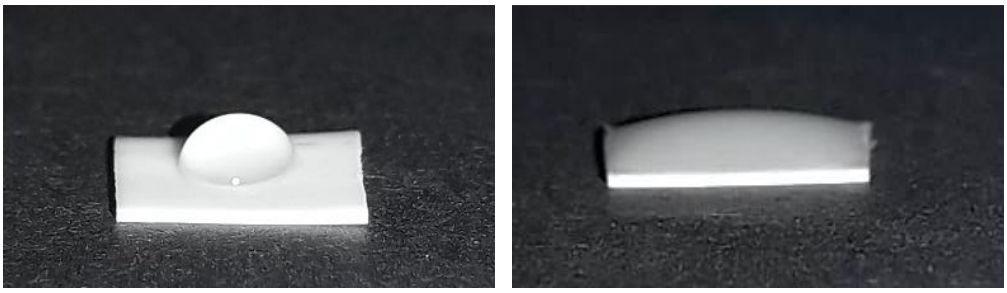

Figure 4.15. Picture of the drops of the drug solution on the surface of IP_LLA films $scCO_2$ processed at SP=10.3 MPa and ST=313 K for S_{time}=24 hours VR=10.9 MPa/min (a) before plasma application (b) after plasma application

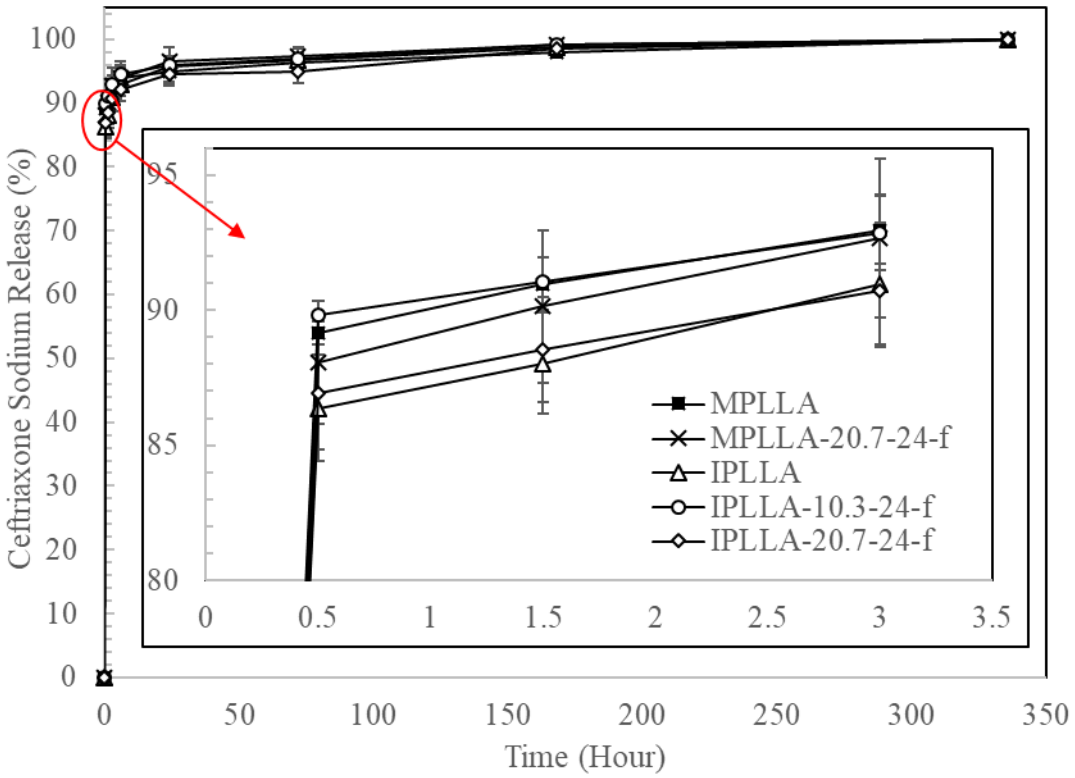

Figure 4.16. Drug release results of the films

CHAPTER 5

CONCLUSIONS

The aim of this study was to obtain porous poly($_L$-lactic acid) (P_LLA) matrices by $scCO_2$ foaming to be used in drug delivery applications. Since it is difficult to obtain porous morphology in a highly crystalline P_LLA matrix (>30%) at moderate temperatures and pressures, CO_2-philic additives were used as pore nucleation agents. Firstly, β-$_D$ galactose pentaacetate (SA) was investigated. In the literature, it was stated that SA formed porous structure after depressurization of SA-CO_2 binary system. Therefore, the foaming ability of SA itself in $scCO_2$ was studied. For this aim, one phase and two-phase system were studied to see if there was a difference. From the results of the foaming experiments, it can be concluded that SA formed fragile structures due to its crystalline morphology. Although some pore-like structures were observed in SEM images, there was no proper pore formation and the microstructure was not porous. Therefore, foaming experiments were carried out with P_LLA.

In order to increase its application area, a pellet form of P_LLA was studied. Pellets were prepared by pressing pure P_LLA powder. To observe the foaming effect of $scCO_2$, this neat P_LLA pellet was processed with $scCO_2$ at 313 K and 20.7 MPa for 24 hours with a depressurization rate of 10.9 MPa/min. These conditions were applied since the best foaming results were obtained in the previous foaming study conducted in our lab with the same polymer. There was no pore formation after the $scCO_2$ processing of the neat P_LLA pellet and the polymer matrix had a heterogeneous structure. This showed that different sample preparation method does not affect the foamability of neat P_LLA at low temperatures. In addition, the pellet was very brittle both before and after processing. After, the pellet was made by mixing P_LLA powder with SA (30 wt %) and wetted with chloroform during pellet making process to keep the matrix integrity, it was processed with $scCO_2$ at 313 K and 20.7 MPa for 24 hours

with a depressurization rate of 10.9 MPa/min. The presence of SA in the matrix resulted in porous structure but the cross-section of pellet and pore distribution were not homogeneous. On the other hand, chloroform helped the pellet keep its integrity. Lastly, to observe the homogeneity in the matrix, instead of SA, SPOSS was used. In order to observe the additive distribution and reproducibility of the pellet, three replicates of P_LLA-SPOSS pellets were prepared. They were made by mixing the powder mixture with chloroform during the pellet preparation to obtain a more homogeneous structure, which is the same method with previous pellet making method. SEM and EDX mapping images showed that the pellet preparation method was not reproducible, and homogeneous cross-section could not be obtained. Therefore, the study was continued with film type of samples.

Solvent-cast neat P_LLA films were processed first to observe the sole effect of $scCO_2$ processing at 313 K and 20.7 MPa for 24 hours with a depressurization rate of 10.9 MPa/min. SEM images showed that there was no pore formation in the matrix after processing which was an expected since same polymer gave the same result when processing with $scCO_2$ at these conditions. In order to increase the affinity of the polymer matrix to CO_2 and make it processable at lower temperatures, SA was used as pore inducer in the P_LLA film with 30 wt %. Addition of SA in P_LLA matrix made the polymer matrix fragile. It may be because of the crystalline structure of the SA. After composite film was processed with $scCO_2$ at 313 K and 20.7 MPa for 24 hours with a depressurization rate of 10.9 MPa/min, homogeneous pore formation was obtained in the matrix cross-section. However, the fragility of the film remained which restricts its usage.

In early mentioned study conducted by Novendra *et al.* in our laboratory, fluorinated POSS (TFPOSS), which was also CO_2-philic, was used; however, the unprocessed P_LLA composite samples and the foamed P_LLA matrices obtained with this additive were highly brittle. So, both in our trials and previous study, using crystalline powder as a nucleating agent resulted in fragile matrices with solvent casting method. In order

to obtain ductile films, two novel CO_2-philic liquid organic-inorganic hybrid components, isooctyl POSS (IPOSS) and methacrylisooctyl POSS (MPOSS) were used as cell nucleators. Addition of these molecules at 10 wt % resulted in the formation of porous polymer matrices even prior to $scCO_2$ processing. Obtained films were ductile. EDX mapping of these composite films showed that POSS distribution in the polymer matrix was homogeneous which resulted in homogeneous pore distribution of films in both processed and unprocessed conditions. Being soluble in CO_2 also allowed the extraction of the POSS molecules from the polymer matrix during the $scCO_2$ processing which is advantageous for recovery and reuse of the expensive cell nucleators. In order to observe the effect of the process parameters systematically, two-level full factorial DoE was used. For the processing of the composite porous films, low and high values of saturation pressure (10.3 and 20.7 MPa), saturation time (2 and 24 hours) and venting rate (0.4 and 10.9 MPa/min) were applied while the saturation temperature kept constant at 313K in the DoE. It was observed that processing at 20.7 MPa for 24 hours of saturation and depressurization with the venting rate of 10.9 MPa/min resulted in increasing of the average pore densities of both composite films from 20.0±1.3 % to 28.8±2.2 % on average. The highest pore density was obtained at this condition for both composite films. The $scCO_2$ processing of the neat P_LLA film at the same condition did not result in the formation of pores in the matrix since it hard to obtain porous structures at low temperatures when crystallinity higher than 30% in neat P_LLA. Pore density of the films decreased with decreasing pressure at constant saturation time and venting rate.

The average pore diameter of the unprocessed MP_LLA film was measured as 1.4±0.3. which was not affected significantly by $scCO_2$ processing or process parameters. The average pore diameter of the processed MP_LLA films was measured as 1.6±0.5 μm. On the other hand, the average pore diameter of the IP_LLA films, which was 3.3±0.6 μm increased 1.6 times and reached to 5.2±1.2 μm when processing at 10.3 MPa for 24 hours regardless of the venting rate. On the other hand, the average pore diameter

decreased with decreasing saturation time. Both pressure and venting rate did not affect the average pore diameter significantly at low saturation time, which was measured as 2.2±0.5 μm. Generally, independent of the processing conditions, all the IP_LLA films had larger average pore diameters than their counterparts with MP_LLA films.

T_g of the neat polymer was measured as 308 K. this low T_g of the polymer can be due to remaining chloroform in the polymer matrix since chloroform acts as plasticizer in the polymer and decreases the intermolecular forces and increases the chain mobility which decreases the T_g of the polymer. T_g of the neat polymer increased with the addition of MPOSS and IPOSS to 312 K and 315 K, respectively, which was in agreement with the literature. Further increase in T_g was observed in all the $scCO_2$-processed films while processing parameters did not affect T_g significantly. Average T_g of all the processed films was calculated as 330±2 K. This can be attributed to removal of the almost all the chloroform during $scCO_2$ processing resulted in more restricted free chain ends. The crystallinity of the neat films did not change either by addition of POSS or $scCO_2$ processing and average crystallinity of all films was measured as 47±1%.

The elastic modulus of the neat polymer increased 1.4 times on average with the addition of POSS into P_LLA due to the reinforcement of the polymer. When the composite films were processed, the elastic modulus of the polymer increased by about 2.6 times compared to the neat polymer. Average moduli of the MP_LLA films and IP_LLA films reached to 1.14 and 1.16 GPa after $scCO_2$ processing, respectively. The percent elongation at break value of P_LLA was found as 290% which is also result of remaining chloroform in the polymer matrix which acts as a plasticizer and increases the ductility of the polymer with increasing the chain mobility. Elongation decreased with the addition of both POSS types which is also observed behavior in the literature that states that using POSS in the P_LLA matrix decrease the polymer ductility. $scCO_2$ processing decreased the % elongation of MP_LLA and IP_LLA films

further. The reasons of this further decrease in the elongation may be the same with those of T_g increase. One of them is realignment of chains locally after $scCO_2$ processing and increasing intermolecular interactions. The other one is the removing of the chloroform after $scCO_2$ foaming which eliminates the plasticizing effect and increase the intermolecular forces.

Drug release studies were performed with Ceftriaxone Sodium, which was used as a model antibiotic. All the films exhibited burst release and about 88±2 % of the loaded drug released in the first 30 minutes, which is followed by a continuous slow release for two weeks. The release behavior is preferable for local antibiotic applications, where an immediate effect on the bacteria is obtained with the burst release and further infection was inhibited with the continuous release of the remaining drug. These film type of matrices can be used in periodontal as well as cancer treatment applications.

Further studies can be performed to increase the usage area of porous P_LLA matrices; the pore sizes and structures, and the density can be altered by mixing multiple types of cell nucleators. Instead of the solvent casting method, different sample preparation methods like melt extruding can be used. Potentials of these porous matrices for other types of applications such as thermal or sound insulation can also be investigated.

REFERENCES

(1) Álvarez-Chávez, C. R.; Edwards, S.; Moure-Eraso, R.; Geiser, K. Sustainability of Bio-Based Plastics: General Comparative Analysis and Recommendations for Improvement. *J. Clean. Prod.* **2012**, *23* (1), 47–56. https://doi.org/10.1016/j.jclepro.2011.10.003.

(2) Babu, R. P.; O'Connor, K.; Seeram, R. Current Progress on Bio-Based Polymers and Their Future Trends. *Prog. Biomater.* **2013**, *2* (1), 8. https://doi.org/10.1186/2194-0517-2-8.

(3) Gupta, B.; Revagade, N.; Hilborn, J. Poly(Lactic Acid) Fiber: An Overview. *Prog. Polym. Sci.* **2007**, *32* (4), 455–482. https://doi.org/10.1016/j.progpolymsci.2007.01.005.

(4) Auras, R.; Harte, B.; Selke, S. An Overview of Polylactides as Packaging Materials. *Macromol. Biosci.* **2004**, *4* (9), 835–864. https://doi.org/10.1002/mabi.200400043.

(5) Bourbigot, S.; Fontaine, G. Flame Retardancy of Polylactide: An Overview. *Polym. Chem.* **2010**, *1* (9), 1413–1422. https://doi.org/10.1039/c0py00106f.

(6) Nofar, M.; Park, C. B. Poly (Lactic Acid) Foaming. *Prog. Polym. Sci.* **2014**, *39* (10), 1721–1741. https://doi.org/10.1016/j.progpolymsci.2014.04.001.

(7) Réti, C.; Casetta, M.; Duquesne, S.; Bourbigot, S.; Delobel, R. Flammability Properties of Intumescent PLA Including Starch and Lignin. *Polym. Adv. Technol.* **2008**, *19* (6), 628–635. https://doi.org/10.1002/pat.1130.

(8) Bettahalli, N. M. S.; Steg, H.; Wessling, M.; Stamatialis, D. Development of Poly(l-Lactic Acid) Hollow Fiber Membranes for Artificial Vasculature in Tissue Engineering Scaffolds. *J. Memb. Sci.* **2011**, *371* (1–2), 117–126. https://doi.org/10.1016/j.memsci.2011.01.026.

(9) da Silva, D.; Kaduri, M.; Poley, M.; Adir, O.; Krinsky, N.; Shainsky-Roitman, J.; Schroeder, A. Biocompatibility, Biodegradation and Excretion of Polylactic Acid (PLA) in Medical Implants and Theranostic Systems. *Chem. Eng. J.* **2018**, *340*, 9–14. https://doi.org/10.1016/j.cej.2018.01.010.

(10) Lasprilla, A. J. R.; Martinez, G. A. R.; Lunelli, B. H.; Jardini, A. L.; Filho, R. M. Poly-Lactic Acid Synthesis for Application in Biomedical Devices - A Review. *Biotechnol. Adv.* **2012**, *30* (1), 321–328. https://doi.org/10.1016/j.biotechadv.2011.06.019.

(11) Okamoto, M.; John, B. Synthetic Biopolymer Nanocomposites for Tissue Engineering Scaffolds. *Prog. Polym. Sci.* **2013**, *38* (10–11), 1487–1503. https://doi.org/10.1016/j.progpolymsci.2013.06.001.

(12) Proikakis, C. S.; Tarantili, P. A.; Andreopoulos, A. G. The Role of Polymer/Drug Interactions on the Sustained Release from Poly(Dl-Lactic Acid) Tablets. *Eur. Polym. J.* **2006**, *42* (12), 3269–3276. https://doi.org/10.1016/j.eurpolymj.2006.08.023.

(13) Saini, P.; Arora, M.; Kumar, M. R. Poly(Lactic Acid) Blends in Biomedical Applications. *Adv. Drug Deliv. Rev.* **2016**, *107*, 47–59. https://doi.org/10.1016/j.addr.2016.06.014.

(14) Eş, I.; Khaneghah, A. M.; Barba, F. J.; Saraiva, J. A.; Sant'Ana, A. S.; Hashemi, S. M. B. Recent Advancements in Lactic Acid Production - a Review. *Food Res. Int.* **2018**, *107*, 763–770. https://doi.org/10.1016/j.foodres.2018.01.001.

(15) Fambri, L.; Migliaresi., C. Crystallization and Thermal Properties. In *Poly (Lactic Acid) Synthesis, Structures, Properties, Processing, and Applications*; 2010; pp 113-124.

(16) Nampoothiri, K. M.; Nair, N. R.; John, R. P. An Overview of the Recent Developments in Polylactide (PLA) Research. *Bioresour. Technol.* **2010**, *101* (22), 8493–8501. https://doi.org/10.1016/j.biortech.2010.05.092.

(17) Kiran, E. Foaming Strategies for Bioabsorbable Polymers in Supercritical Fluid Mixtures. Part I. Miscibility and Foaming of Poly (l-Lactic Acid) in Carbon Dioxide+acetone Binary Fluid Mixtures. *J. Supercrit. Fluids* **2010**, *54* (3), 296–307. https://doi.org/10.1016/j.supflu.2010.05.005.

(18) Hamad, K.; Kaseem, M.; Yang, H. W.; Deri, F.; Ko, Y. G. Properties and Medical Applications of Polylactic Acid: A Review. *Express Polym. Lett.* **2015**, *9* (5). https://doi.org/10.3144/expresspolymlett.2015.42.

(19) Woodland, J. H. R.; Yolles, S.; Blake, D. A.; Helrich, M.; Meyer, F. J. Long-Acting Delivery Systems for Narcotic Antagonists. 1. *J. Med. Chem.* **1973**, *16* (8), 897–901. https://doi.org/10.1021/jm00266a007.

(20) Yolles, S.; Leafe, T. D.; H.R.Woodland, J.; J.Meyer, F. Long Acting Delivery Systems for Narcotic Antagonists II: Release Rates of Naltrexone from Poly(Lactic Acid) Composites. *J. Pharm. Sci.* **1975**, *64* (2), 348–349. https://doi.org/https://doi.org/10.1002/jps.2600640239.

(21) Krukiewicz, K.; Zak, J. K. Biomaterial-Based Regional Chemotherapy: Local Anticancer Drug Delivery to Enhance Chemotherapy and Minimize Its Side-Effects. *Mater. Sci. Eng. C* **2016**, *62*, 927–942. https://doi.org/10.1016/j.msec.2016.01.063.

(22) Perugini, P.; Genta, I.; Conti, B.; Modena, T.; Pavanetto, F. Periodontal Delivery of Ipriflavone: New Chitosan/PLGA Film Delivery System for a Lipophilic Drug. *Int. J. Pharm.* **2003**, *252* (1–2), 1–9. https://doi.org/10.1016/S0378-5173(02)00602-6.

(23) Liao, X.; Zhang, H.; He, T. Preparation of Porous Biodegradable Polymer and Its Nanocomposites by Supercritical CO 2 Foaming for Tissue Engineering. *J. Nanomater.* **2012**, *2012*, 6. https://doi.org/10.1155/2012/836394.

(24) Zhang, X.; Heinonen, S.; Levänen, E. Applications of Supercritical Carbon Dioxide in Materials Processing and Synthesis. *RSC Adv.* **2014**, *4* (105), 61137–61152. https://doi.org/10.1039/c4ra10662h.

(25) Duarte, A. R. C.; Mano, J. F.; Reis, R. L. Perspectives on: Supercritical Fluid Technology for 3D Tissue Engineering Scaffold Applications. *J. Bioact. Compat. Polym.* **2009**, *24* (4), 385–400. https://doi.org/10.1177/0883911509105796.

(26) Duarte, A. R. C.; Santo, V. E.; Alves, A.; Silva, S. S.; Moreira-Silva, J.; Silva, T. H.; Marques, A. P.; Sousa, R. A.; Gomes, M. E.; Mano, J. F.; et al. Unleashing the Potential of Supercritical Fluids for Polymer Processing in Tissue Engineering and Regenerative Medicine. *J. Supercrit. Fluids* **2013**, *79*, 177–185. https://doi.org/10.1016/j.supflu.2013.01.004.

(27) White, L. J.; Hutter, V.; Tai, H.; Howdle, S. M.; Shakesheff, K. M. The Effect of Processing Variables on Morphological and Mechanical Properties of Supercritical CO2 Foamed Scaffolds for Tissue Engineering. *Acta Biomater.* **2012**, *8* (1), 61–71. https://doi.org/10.1016/j.actbio.2011.07.032.

(28) García-González, C. A.; Concheiro, A.; Alvarez-Lorenzo, C. Processing of Materials for Regenerative Medicine Using Supercritical Fluid Technology. *Bioconjug. Chem.* **2015**, *26* (7), 1159–1171. https://doi.org/10.1021/bc5005922.

(29) Gualandi, C.; White, L. J.; Chen, L.; Gross, R. A.; Shakesheff, K. M.; Howdle, S. M.; Scandola, M. Scaffold for Tissue Engineering Fabricated by Non-Isothermal Supercritical Carbon Dioxide Foaming of a Highly Crystalline Polyester. *Acta Biomater.* **2010**, *6* (1), 130–136. https://doi.org/10.1016/j.actbio.2009.07.020.

(30) Mikos, A. G.; Temenoff, J. S. Formation of Porous Biodegradable Scaffolds for Tissue Engineering. *Electron. J. Biotechnol.* **2000**, *3* (2), 23–24. https://doi.org/10.4067/s0717-34582000000200003.

(31) Janik, H.; Marzec, M. A Review: Fabrication of Porous Polyurethane Scaffolds. *Mater. Sci. Eng. C* **2015**, *48*, 586–591. https://doi.org/10.1016/j.msec.2014.12.037.

(32) Sachlos, E.; Czernuszka, J. T. Making Tissue Engineering Scaffolds Work. Review on the Application of Solid Freeform Fabrication Technology to the Production of Tissue Engineering Scaffolds. *Eur. Cells Mater.* **2003**, *5* (29), 39–40. https://doi.org/10.22203/eCM.v005a03.

(33) Ghosh, S.; Viana, J. C.; Reis, R. L.; Mano, J. F. The Double Porogen Approach as a New Technique for the Fabrication of Interconnected Poly(L-Lactic Acid) and Starch Based Biodegradable Scaffolds. *J. Mater. Sci. Mater. Med.* **2007**, *18* (2), 185–193. https://doi.org/10.1007/s10856-006-0680-y.

(34) Kim, J. F.; Kim, J. H.; Lee, Y. M. Thermally Induced Phase Separation and Electrospinning Methods for Emerging Membrane Applications: A Review. *AIChE J.* **2016**, *62* (2), 461–490. https://doi.org/10.1002/aic.15076.

(35) Ahmed, F. E.; Lalia, B. S.; Hashaikeh, R. A Review on Electrospinning for Membrane Fabrication: Challenges and Applications. *Desalination* **2015**, *356*, 15–30. https://doi.org/10.1016/j.desal.2014.09.033.

(36) Cooper, A. I. Porous Materials and Supercritical Fluids. *Adv. Mater.* **2003**, *15* (13), 1049–1059. https://doi.org/10.1002/adma.200300380.

(37) Lim, L. T.; Auras, R.; Rubino, M. Processing Technologies for Poly(Lactic Acid). *Prog. Polym. Sci.* **2008**, *33* (8), 820–852. https://doi.org/10.1016/j.progpolymsci.2008.05.004.

(38) Novendra, N.; Hasirci, N.; Dilek, C. Supercritical Processing of CO2-Philic Polyhedral Oligomeric Silsesquioxane (POSS)-Poly(L-Lactic Acid) Composites. *J. Supercrit. Fluids* **2016**, *117*, 230–242. https://doi.org/10.1016/j.supflu.2016.06.022.

(39) Rouholamin, D.; Smith, P. J.; Ghassemieh, E. Control of Morphological Properties of Porous Biodegradable Scaffolds Processed by Supercritical CO2 Foaming. *J. Mater. Sci.* **2013**, *48* (8), 3254–3263. https://doi.org/10.1007/s10853-012-7109-4.

(40) Davies, O. R.; Lewis, A. L.; Whitaker, M. J.; Tai, H.; Shakesheff, K. M.; Howdle, S. M. Applications of Supercritical CO2 in the Fabrication of Polymer Systems for Drug Delivery and Tissue Engineering. *Adv. Drug Deliv. Rev.* **2008**, *60* (3), 373–387. https://doi.org/10.1016/j.addr.2006.12.001.

(41) Oliveira, N. S.; Dorgan, J.; Coutinho, J. A. P.; Ferreira, A.; Daridon, J. L.; Marrucho, I. M. Gas Solubility of Carbon Dioxide in Poly(Lactic Acid) at High Pressures: Thermal Treatment Effect. *J. Polym. Sci. Part B Polym. Phys.* **2007**, *45* (5), 616–625. https://doi.org/10.1002/polb.20969.

(42) Pini, R.; Storti, G.; Mazzotti, M.; Tai, H.; Shakesheff, K. M.; Howdle, S. M. Sorption and Swelling of Poly(DL-Lactic Acid) and Poly(Lactic-Co-Glycolic Acid) in Supercritical CO2: An Experimental and Modeling Study. *J. Polym. Sci. Part B Polym. Phys.* **2008**, *46* (5), 483–496. https://doi.org/10.1002/polb.21382.

(43) Aionicesei, E.; Škerget, M.; Knez, Ž. Measurement of CO2 Solubility and Diffusivity in Poly(l-Lactide) and Poly(d,l-Lactide-Co-Glycolide) by Magnetic Suspension Balance. *J. Supercrit. Fluids* **2008**, *47* (2), 296–301. https://doi.org/10.1016/j.supflu.2008.07.011.

(44) Jinpeng, Y. U.; Chuan, T. A. N. G.; Yixin, G. U. A. N.; Shanjing, Y. A. O.; Ziqiang, Z. H. O. Sorption and Diffusion Behavior of Carbon Dioxide into Poly(l-Lactic Acid) Films at Elevated Pressures. *Chinese J. Chem. Eng.* **2013**, *21* (11), 1296–1302. https://doi.org/10.1016/S1004-9541(13)60623-0.

(45) Baldwin, D. F.; Shimbo, M.; Suh, N. P. The Role of Gas Dissolution and Induced Crystallization During Microcellular Polymer Processing: A Study of Poly (Ethylene Terephthalate) and Carbon Dioxide Systems. *J. Eng. Mater. Technol.* **1995**, *117* (1), 62–74. https://doi.org/10.1115/1.2804373.

(46) Liao, X.; Nawaby, A. V.; Whitfield, P. S. Carbon Dioxide-Induced Crystallization in Poly(L-Lactic Acid) and Its Effect on Foam Morphologies. *Polym. Int.* **2010**, *59* (12), 1709–1718. https://doi.org/10.1002/pi.2910.

(47) Taki, K.; Kitano, D.; Ohshima, M. Effect of Growing Crystalline Phase on Bubble Nucleation in Poly(L-Lactide)/CO2 Batch Foaming. *Ind. Eng. Chem. Res.* **2011**, *50* (6), 3247–3252. https://doi.org/10.1021/ie101637f.

(48) López-Periago, A. M.; Vega, A.; Subra, P.; Argemí, A.; Saurina, J.; García-González, C. A.; Domingo, C. Supercritical CO2 Processing of Polymers for the Production of Materials with Applications in Tissue Engineering and Drug Delivery. *J. Mater. Sci.* **2008**, *43* (6), 1939–1947. https://doi.org/10.1007/s10853-008-2461-0.

(49) Mathieu, L. M.; Montjovent, M. O.; Bourban, P. E.; Pioletti, D. P.; Månson, J. A. E. Bioresorbable Composites Prepared by Supercritical Fluid Foaming. *J. Biomed. Mater. Res. - Part A* **2005**, *75* (1), 89–97. https://doi.org/10.1002/jbm.a.30385.

(50) Delabarde, C.; Plummer, C. J. G.; Bourban, P. E.; Månson, J. A. E. Biodegradable Polylactide/Hydroxyapatite Nanocomposite Foam Scaffolds for Bone Tissue Engineering Applications. *J. Mater. Sci. Mater. Med.* **2012**, *23* (6), 1371–1385. https://doi.org/10.1007/s10856-012-4619-1.

(51) Georgiou, G.; Mathieu, L.; Pioletti, D. P.; Bourban, P. E.; Månson, J. A.; Knowles, J. C.; Nazhat., S. N. Polylactic Acid–Phosphate Glass Composite Foams as Scaffolds for Bone Tissue Engineering. *J. Biomed. Mater. Res. B. Appl. Biomater.* **2007**, *80* (2), 322–331. https://doi.org/10.1002/jbm.b.30600.

(52) Costeux, S.; Zhu, L. Low Density Thermoplastic Nanofoams Nucleated by Nanoparticles. *Polymer (Guildf).* **2013**, *54* (11), 2785–2795. https://doi.org/10.1016/j.polymer.2013.03.052.

(53) Wang, C.; Leung, S. N.; Bussmann, M.; Zhai, W. T.; Park, C. B. Numerical Investigation of Nucleating-Agent-Enhanced Heterogeneous Nucleation. *Ind. Eng. Chem. Res.* **2010**, *49* (24), 12783–12792. https://doi.org/10.1021/ie1017207.

(54) Di Maio, E.; Kiran, E. Foaming of Polymers with Supercritical Fluids and

Perspectives on the Current Knowledge Gaps and Challenges. *J. Supercrit. Fluids* **2018**, *134*, 157–166. https://doi.org/10.1016/j.supflu.2017.11.013.

(55) He, Z.; Zhong, M.; Yang, Y.; Wu, C.; Yang, J. Synthesis of POSS-Based Star-Shaped Poly(Ionic Liquid)s and Its Application in Supercritical CO2 Microcellular Foaming of Polystyrene. *J. Polym. Res.* **2016**, *23* (12), 243. https://doi.org/10.1007/s10965-016-1142-y.

(56) Ghanbari, H.; Marashi, S. M.; Rafiei, Y.; Chaloupka, K.; Seifalian, A. M. Biomedical Application of Polyhedral Oligomeric Silsesquioxane Nanoparticles. In *Applications of polyhedral oligomeric silsesquioxanes*; Springer, Dordrecht, 2011; pp 363–399. https://doi.org/10.1007/978-90-481-3787-9_9.

(57) Carroll, J. B.; Waddon, A. J.; Nakade, H.; Rotello, V. M. "Plug and Play" Polymers. Thermal and X-Ray Characterizations of Noncovalently Grafted Polyhedral Oligomeric Silsesquioxane (POSS)−Polystyrene Nanocomposites. *Macromolecules* **2003**, *36* (17), 6289–6291. https://doi.org/10.1021/ma034652u.

(58) McCusker, C.; Carroll, J. B.; Rotelo, V. M. Cationic Polyhedral Oligomeric Silsesquioxane (POSS) Units as Carriers for Drug Delivery Processes. *Chem. Commun.* **2005**, No. 8, 996–998. https://doi.org/10.1039/b416266h.

(59) Zheng, L.; Farris, R. J.; Coughlin, E. B. Novel Polyolefin Nanocomposites: Synthesis and Characterizations of Metallocene-Catalyzed Polyolefin Polyhedral Oligomeric Silsesquioxane Copolymers. *Macromolecules* **2001**, *34* (23), 8034–8039. https://doi.org/10.1021/ma0110094.

(60) Kim, S. K.; Heo, S. J.; Koak, J. Y.; Lee, J. H.; Lee, Y. M.; Chung, D. J.; Lee, J. I.; Hong, S. D. A Biocompatibility Study of a Reinforced Acrylic-Based Hybrid Denture Composite Resin with Polyhedraloligosilsesquioxane. *J. Oral Rehabil.* **2007**, *34* (5), 389–395. https://doi.org/10.1111/j.1365-2842.2006.01671.x.

(61) Gao, F.; Tong, Y.; Schricker, S. R.; Culbertson, B. M. Evaluation of Neat

Resins Based on Methacryplates Modified with Methacryl-POSS, as Potential Organic-Inorganic Hybrids for Formulating Dental Restoratives. *Polym. Adv. Technol.* **2001**, *12* (6), 355–360. https://doi.org/10.1002/pat.117.

(62) Dodiuk-Kenig, H.; Maoz, Y.; Lizenboim, K.; Eppelbaum, I.; Zalsman, B.; Kenig, S. The Effect of Grafted Caged Silica (Polyhedral Oligomeric Silesquioxanes) on the Properties of Dental Composites and Adhesives. *J. Adhes. Sci. Technol.* **2006**, *20* (12), 1401–1412. https://doi.org/10.1163/156856106778456609.

(63) Zou, Q. C.; Yan, Q. J.; Song, G. W.; Zhang, S. L.; Wu, L. M. Detection of DNA Using Cationic Polyhedral Oligomeric Silsesquioxane Nanoparticles as the Probe by Resonance Light Scattering Technique. *Biosens. Bioelectron.* **2007**, *22* (7), 1461–1465. https://doi.org/10.1016/j.bios.2006.06.028.

(64) Kidane, A. G.; Burriesci, G.; Edirisinghe, M.; Ghanbari, H.; Bonhoeffer, P.; Seifalian, A. M. A Novel Nanocomposite Polymer for Development of Synthetic Heart Valve Leaflets. *Acta Biomater.* **2009**, *5* (7), 2409–2417. https://doi.org/10.1016/j.actbio.2009.02.025.

(65) Gupta, A.; Seifalian, A. M.; Ahmad, Z.; Edirisinghe, M. J.; Winslet, M. C. Novel Electrohydrodynamic Printing of Nanocomposite Biopolymer Scaffolds. *J. Bioact. Compat. Polym.* **2007**, *22* (3), 265–280. https://doi.org/10.1177/0883911507078268.

(66) Gupta, A.; Vara, D. S.; Punshon, G.; Sales, K. M.; Winslet, M. C.; Seifalian, A. M. In Vitro Small Intestinal Epithelial Cell Growth on a Nanocomposite Polycaprolactone Scaffold . *Biotechnol. Appl. Biochem.* **2009**, *54* (4), 221–229. https://doi.org/10.1042/ba20090214.

(67) Raghunath, J.; Zhang, H.; Edirisinghe, M. J.; Darbyshire, A.; Butler, P. E.; Seifalian, A. M. A New Biodegradable Nanocomposite Based on Polyhedral Oligomeric Silsesquioxane Nanocages: Cytocompatibility and Investigation into Electrohydrodynamic Jet Fabrication Techniques for Tissue-Engineered Scaffolds. *Biotechnol. Appl. Biochem.* **2009**, *52* (1), 1–8. https://doi.org/10.1042/ba20070256.

(68) Dilek, C. Supercritical Carbon Dioxide-Soluble Polyhedral Oligomeric Silsesquioxane (POSS) Nanocages and Polymer Surface Modification. *J. Supercrit. Fluids* **2013**, *73*, 171–177. https://doi.org/10.1016/j.supflu.2012.10.012.

(69) Kanya, B.; Dilek, C. Effects of Functional Groups on the Solubilities of Polyhedral Oligomeric Silsesquioxanes (POSS) in Supercritical Carbon Dioxide. *J. Supercrit. Fluids* **2015**, *102*, 17–23. https://doi.org/10.1016/j.supflu.2015.03.024.

(70) Potluri, V. K.; Xu, J.; Enick, R.; Beckman, E.; Hamilton, A. D. Peracetylated Sugar Derivatives Show High Solubility in Liquid and Supercritical Carbon Dioxide. *Org. Lett.* **2002**, *4* (14), 2333–2335. https://doi.org/10.1021/ol026007y.

(71) Raveendran, P.; Wallen, S. L. Sugar Acetates as Novel, Renewable CO2-Philes. *J. Am. Chem. Soc.* **2002**, *124* (25), 7274–7275. https://doi.org/10.1021/ja025508b.

(72) Dilek, C.; Manke, C. W.; Gulari, E. Phase Behavior of β-d Galactose Pentaacetate-Carbon Dioxide Binary System. *Fluid Phase Equilib.* **2006**, *239* (2), 172–177. https://doi.org/10.1016/j.fluid.2005.11.013.

(73) Demirtas, C.; Dilek, C. Enhanced Solubility of Siloxy-Modified Polyhedral Oligomeric Silsesquioxanes in Supercritical Carbon Dioxide. *J. Supercrit. Fluids* **2019**, *143*, 358–364. https://doi.org/https://doi.org/10.1016/j.supflu.2018.09.015.

(74) Dumanlilar, B.; Demirtas, C.; Dilek, C. Enhancing the CO2-Philicity of Organic-Inorganic Hybrid Polyhedral Oligomeric Silsesquioxanes. In *17th European Meeting on Supercritical Fluids (EMSF 2019) - 7th European Meeting on High Pressure Technology*; Real, Spain, 2019.

(75) Lee, T. H.; Boey, F. Y. C.; Khor, K. A. On the Determination of Polymer Crystallinity for a Thermoplastic PPS Composite by Thermal Analysis.

Compos. Sci. Technol. **1995**, *53* (3), 259–274. https://doi.org/10.1016/0266-3538(94)00070-0.

(76) Fischer, E. W.; Sterzel, H. J.; Wegner, G. Investigation of the Structure of Solution Grown Crystals of Lactide Copolymers. *Kolloid-Zeitschrift und Zeitschrift für Polym.* **1973**, *251* (11), 980–990. https://doi.org/10.1007/BF01498927.

(77) Zhang, H.; Long, J.; Cooper, A. I. Aligned Porous Materials by Directional Freezing of Solutions in Liquid CO2. *J. Am. Chem. Soc.* **2005**, *127* (39), 13482–13483. https://doi.org/10.1021/ja054353f.

(78) Rhim, J. W.; Mohanty, A. K.; Singh, S. P.; Ng, P. K. W. Effect of the Processing Methods on the Performance of Polylactide Films: Thermocompression versus Solvent Casting. *J. Appl. Polym. Sci.* **2006**, *101* (6), 3736–3742. https://doi.org/10.1002/app.23403.

(79) Farah, S.; Anderson, D. G.; Langer, R. Physical and Mechanical Properties of PLA, and Their Functions in Widespread Applications — A Comprehensive Review. *Adv. Drug Deliv. Rev.* **2016**, *107*, 367–392. https://doi.org/10.1016/j.addr.2016.06.012.

(80) Rhim, J. W.; Hong, S. I.; Ha, C. S. Tensile, Water Vapor Barrier and Antimicrobial Properties of PLA/Nanoclay Composite Films. *LWT - Food Sci. Technol.* **2009**, *42* (2), 612–617. https://doi.org/10.1016/j.lwt.2008.02.015.

(81) Chakoli, A. N.; He, J.; Chayjan, M. A.; Huang, Y.; Zhang, B. Irradiation of Poly(l-Lactide) Biopolymer Reinforced with Functionalized MWCNTs. *RSC Adv.* **2015**, *5* (68), 55544–55549. https://doi.org/10.1039/c5ra08319b.

(82) Fernández, M. D.; Fernández, M. J.; Cobos, M. Effect of Polyhedral Oligomeric Silsesquioxane (POSS) Derivative on the Morphology, Thermal, Mechanical and Surface Properties of Poly(Lactic Acid)-Based Nanocomposites. *J. Mater. Sci.* **2016**, *51* (7), 3628–3642. https://doi.org/10.1007/s10853-015-9686-5.

(83) Ferreira, B. M. P.; Pinheiro, L. M. P.; Nascente, P. A. P.; Ferreira, M. J.; Duek, E. A. R. Plasma Surface Treatments of Poly(l-Lactic Acid) (PLLA) and Poly(Hydroxybutyrate-Co-Hydroxyvalerate) (PHBV). *Mater. Sci. Eng. C* **2009**, *29* (3), 806–813. https://doi.org/10.1016/j.msec.2008.07.026.

(84) Hasirci, V.; Tezcaner, A.; Hasirci, N.; Suzer, S. Oxygen Plasma Modification of Poly (3-Hydroxy Butyrate-Co-3-Hydroxyvalerate) Film Surfaces for Tissue Engineering Purposes. *J. Appl. Polym. Sci.* **2003**, *87* (8), 1285–1289. https://doi.org/10.1002/app.11532.

(85) Ozcan, C.; N. Hasirci. Evaluation of Surface Free Energy for PMMA Films. *J. Appl. Polym. Sci.* **2008**, *108* (1), 438–446. https://doi.org/10.1002/app.27687.

(86) Ozgen, O.; Aksoy, E. A.; Hasirci, V.; Hasirci, N. Surface Characterization and Radical Decay Studies of Oxygen Plasma Treated PMMA Films, Surface and Interface Analysis. *Surf. Interface Anal.* **2013**, *45* (4), 844–853. https://doi.org/10.1002/sia.5181.

APPENDICES

A. SEM Images of Processed Samples

Labeling of the processed samples were denoted as SP-S_{time}-VR, where SP is the saturation pressure (10.3 or 20.7 MPa), S_{time} is the saturation time (2 or 24 hours) and VR is the venting rate (0.4 or 10.9 MPa/min as slow (s) or fast (f), respectively))

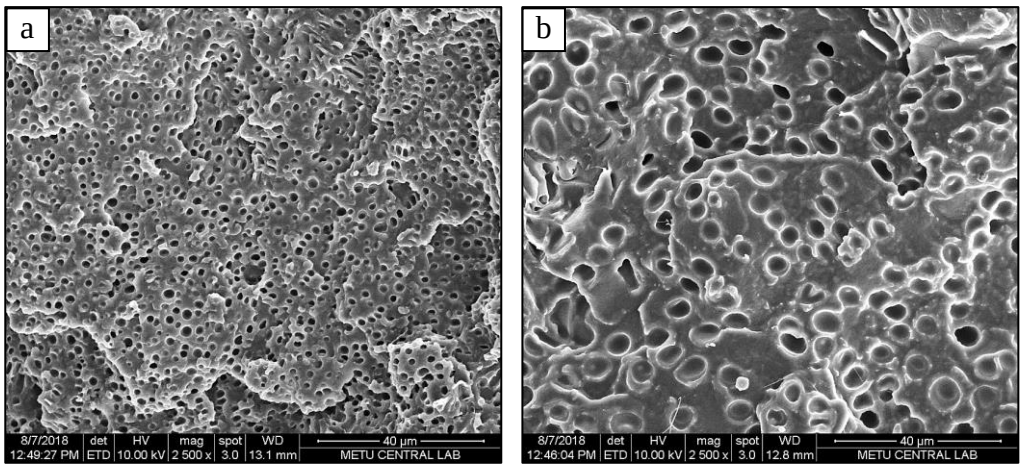

Figure 0.1. SEM images of the cross-section of (a) MP_LLA-10.3-24-f (b) IP_LLA-10.3-24-f (scale bar=40 µm for both images)

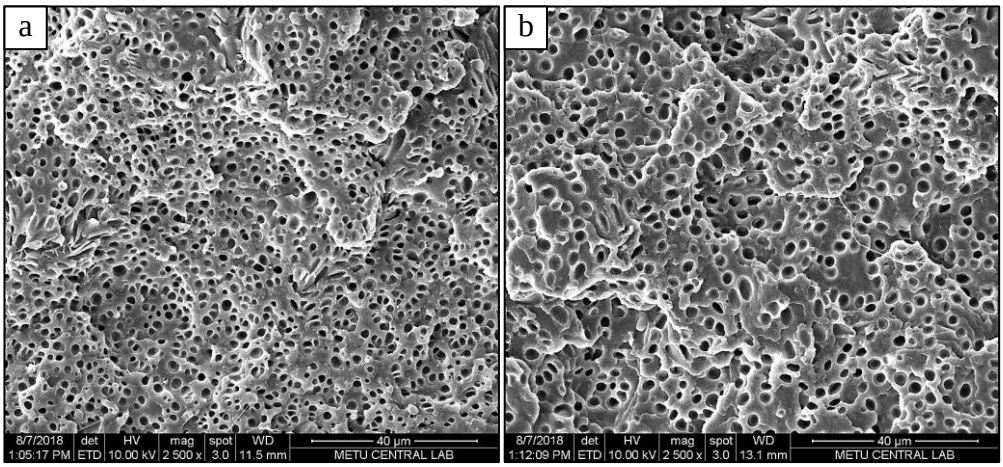

Figure 0.2. SEM images of the cross-section of (a) MP_LLA-20.7-24-s (b) IP_LLA-20.7-24-s (scale bar=40 µm for both images)

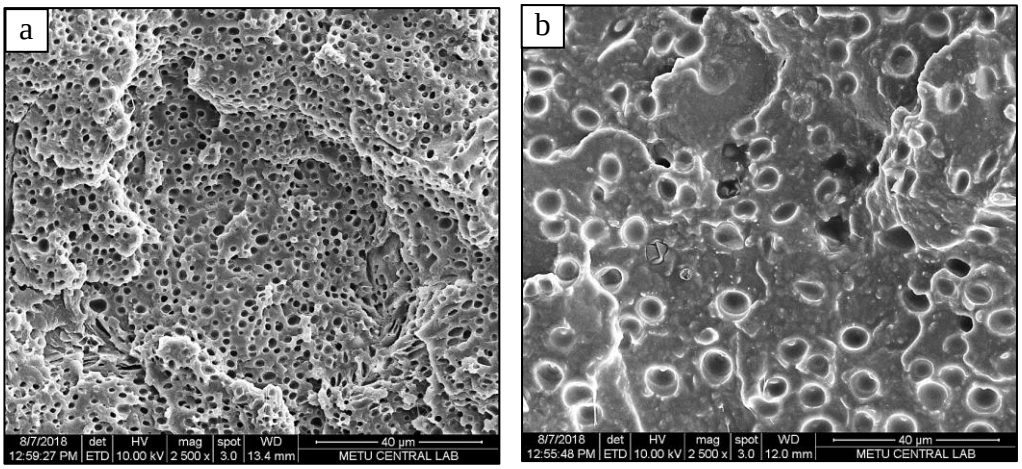

Figure 0.3. SEM images of the cross-section of (a) MP_LLA-10.3-24-s (b) IP_LLA-10.3-24-s (scale bar=40 µm for both images)

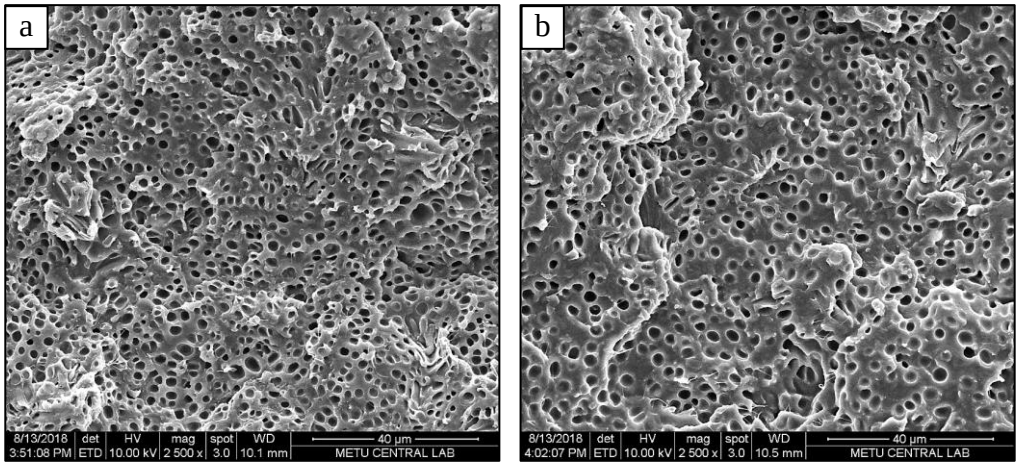

Figure 0.4. SEM images of the cross-section of (a) MP_LLA-20.7-2-f (b) IP_LLA-20.7-2-f (scale bar=40 µm for both images)

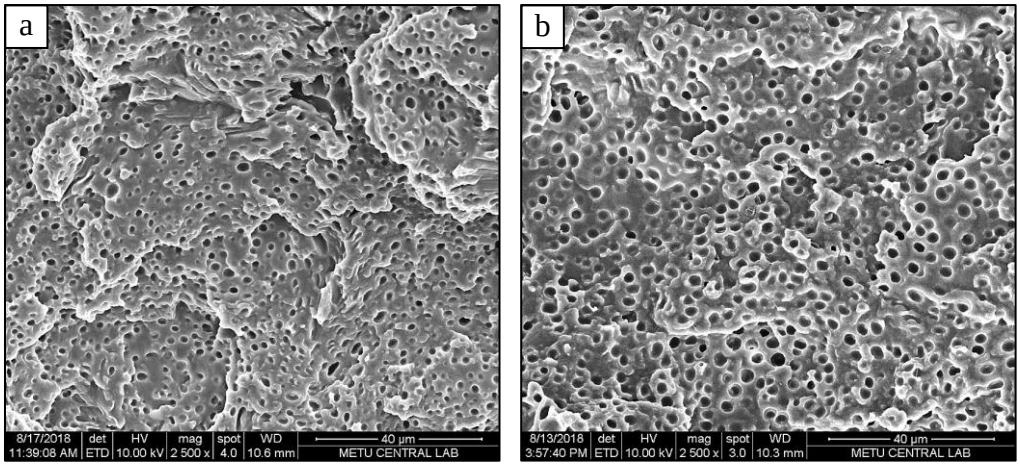

Figure 0.5. SEM images of the cross-section of (a) MP_LLA-10.3-2-f (b) IP_LLA-10.3-2-f (scale bar=40 µm for both images)

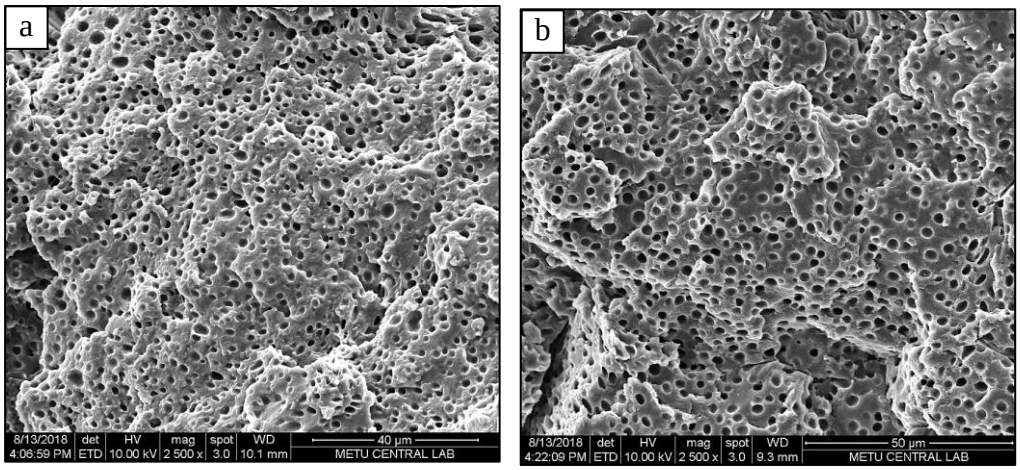

Figure 0.6. SEM images of the cross-section of (a) MP_LLA-20.7-2-s (scale bar=40) (b) IP_LLA-20.7-2-s (scale bar=50 µm)

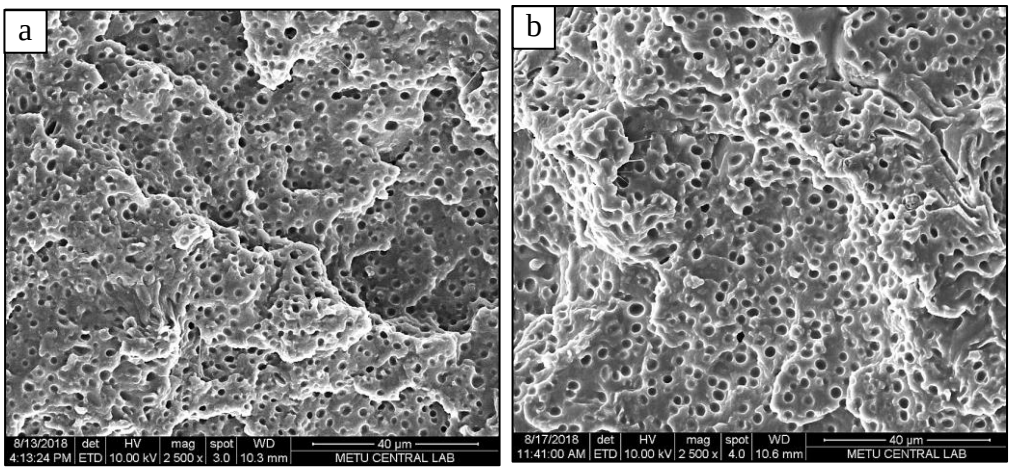

Figure 0.7. SEM images of the cross-section of (a) MP_LLA-10.3-2-s (b) IP_LLA-10.3-2-s (scale bar=40 µm for both images)

B. DSC Thermograms

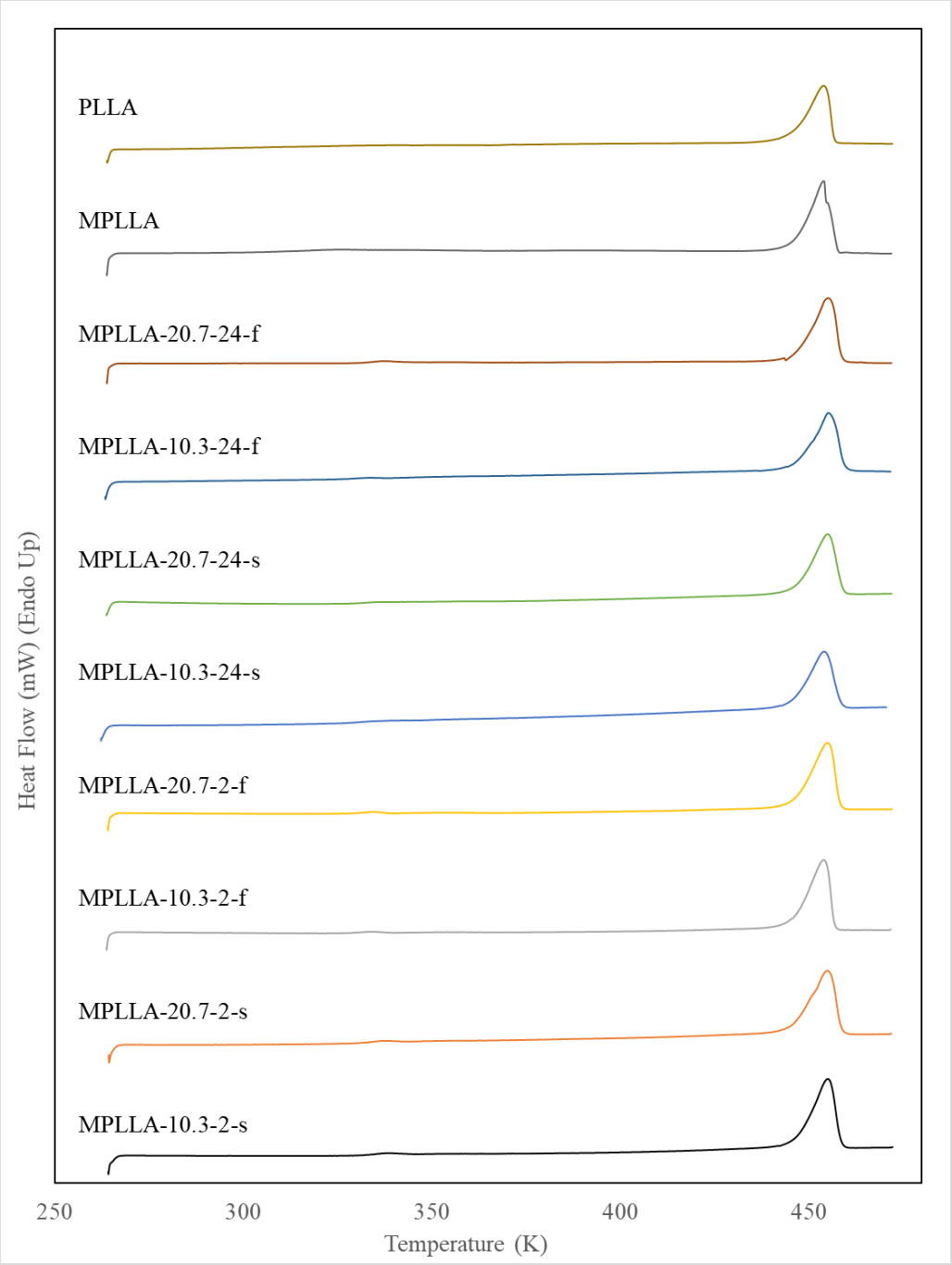

Figure 0.8. First heating DSC thermogram of MP_LLA films (Labeling of the processed samples were denoted as SP-S_{time}-VR, where SP is the saturation pressure (10.3 or 20.7 MPa), S_{time} is the saturation time (2 or 24 hours) and VR is the venting rate (0.4 or 10.9 MPa/min as slow (s) or fast (f), respectively))

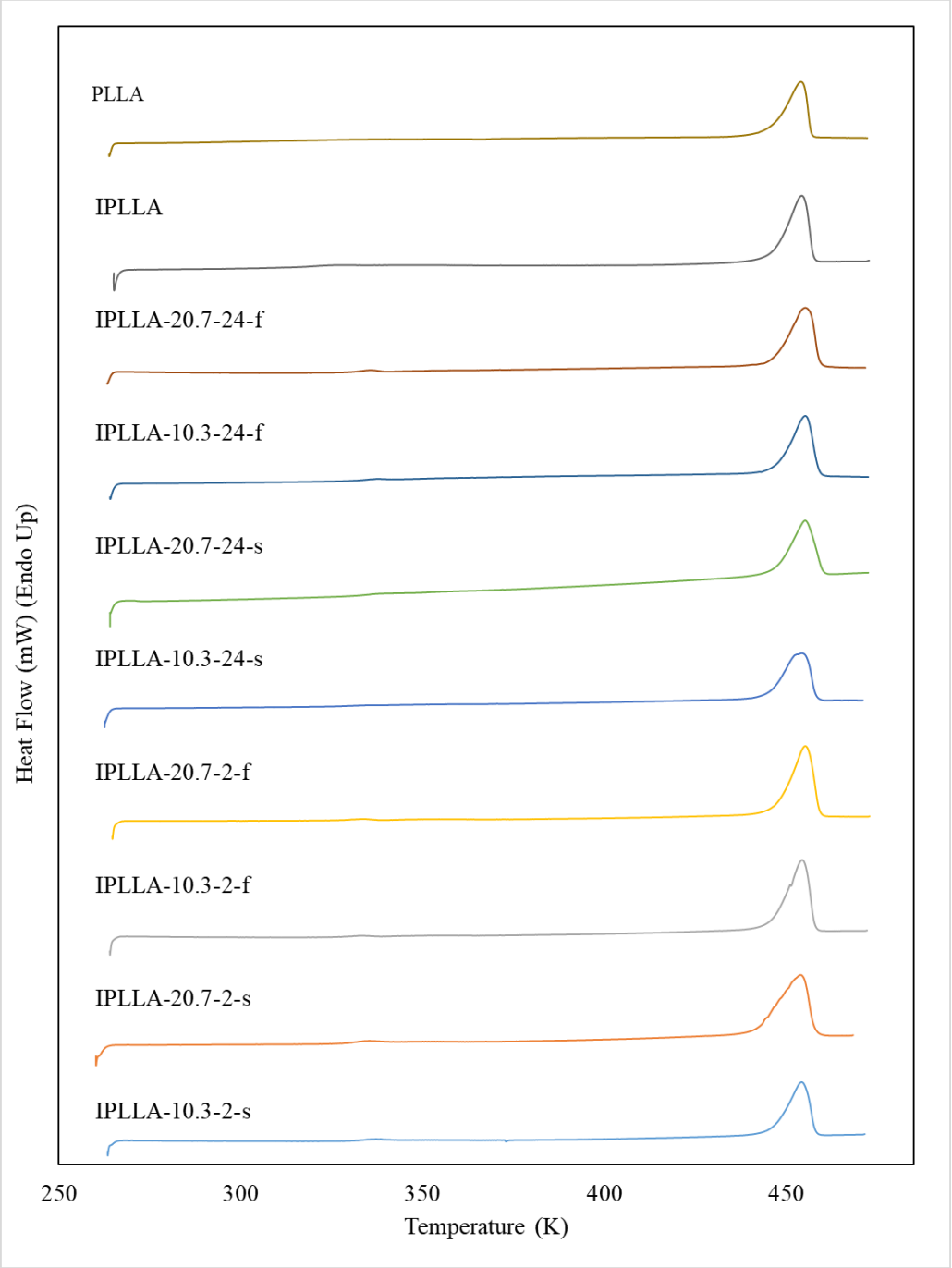

Figure 0.9. First heating DSC thermogram of IP$_L$LA films (Labeling of the processed samples were denoted as SP-S$_{time}$-VR, where SP is the saturation pressure (10.3 or 20.7 MPa), S$_{time}$ is the saturation time (2 or 24 hours) and VR is the venting rate (0.4 or 10.9 MPa/min as slow (s) or fast (f), respectively))

C. EDX Analyses

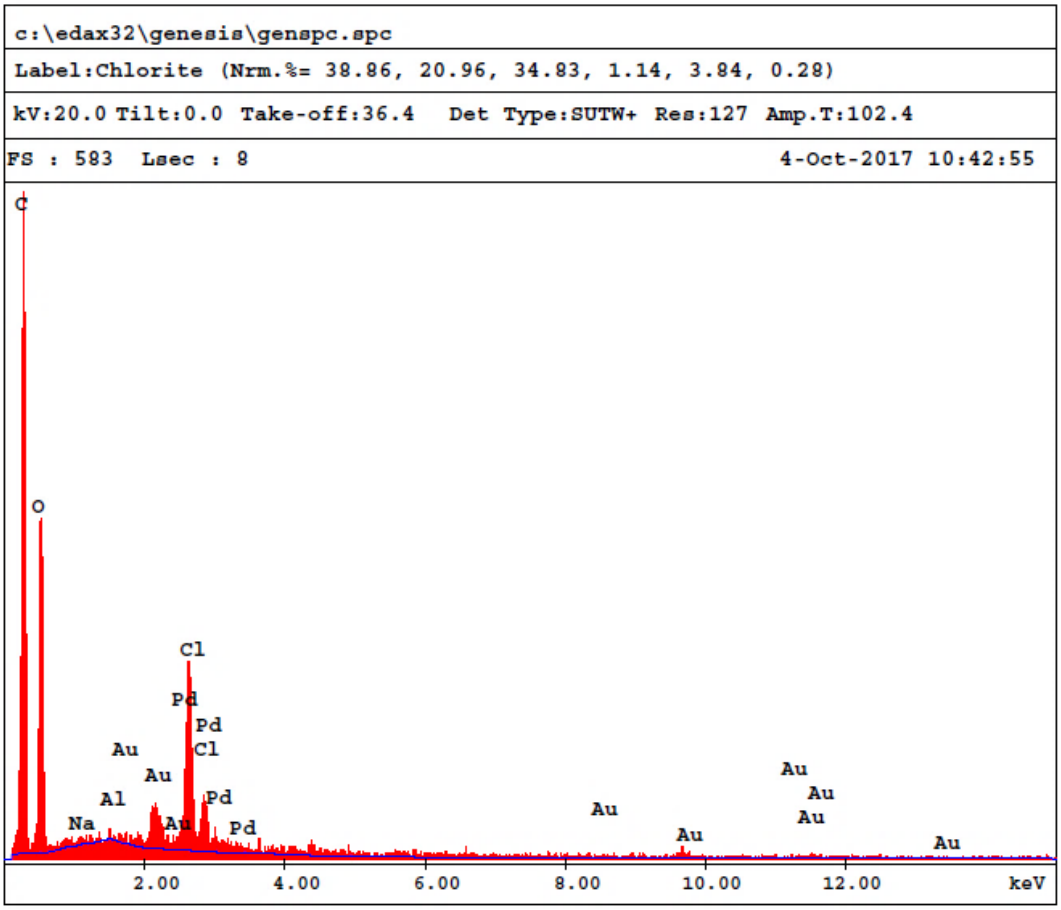

EDAX ZAF Quantification (Standardless)
Element Normalized
SEC Table : Default

Element	Wt %	At %	K-Ratio	Z	A	F
C K	61.60	73.90	0.2349	1.0246	0.3722	1.0002
O K	26.17	23.57	0.0467	1.0075	0.1773	1.0000
NaK	0.00	0.00	0.0000	0.9431	0.4264	1.0003
AlK	0.00	0.00	0.0000	0.9386	0.7303	1.0012
ClK	4.42	1.80	0.0383	0.9078	0.9516	1.0031
PdL	2.50	0.34	0.0205	0.7607	1.0777	1.0000
AuL	5.31	0.39	0.0345	0.6260	1.0380	1.0000
Total	100.00	100.00				

Figure 0.10. EDX analysis of the cross-section of the entire thickness of the unprocessed neat P_LLA films

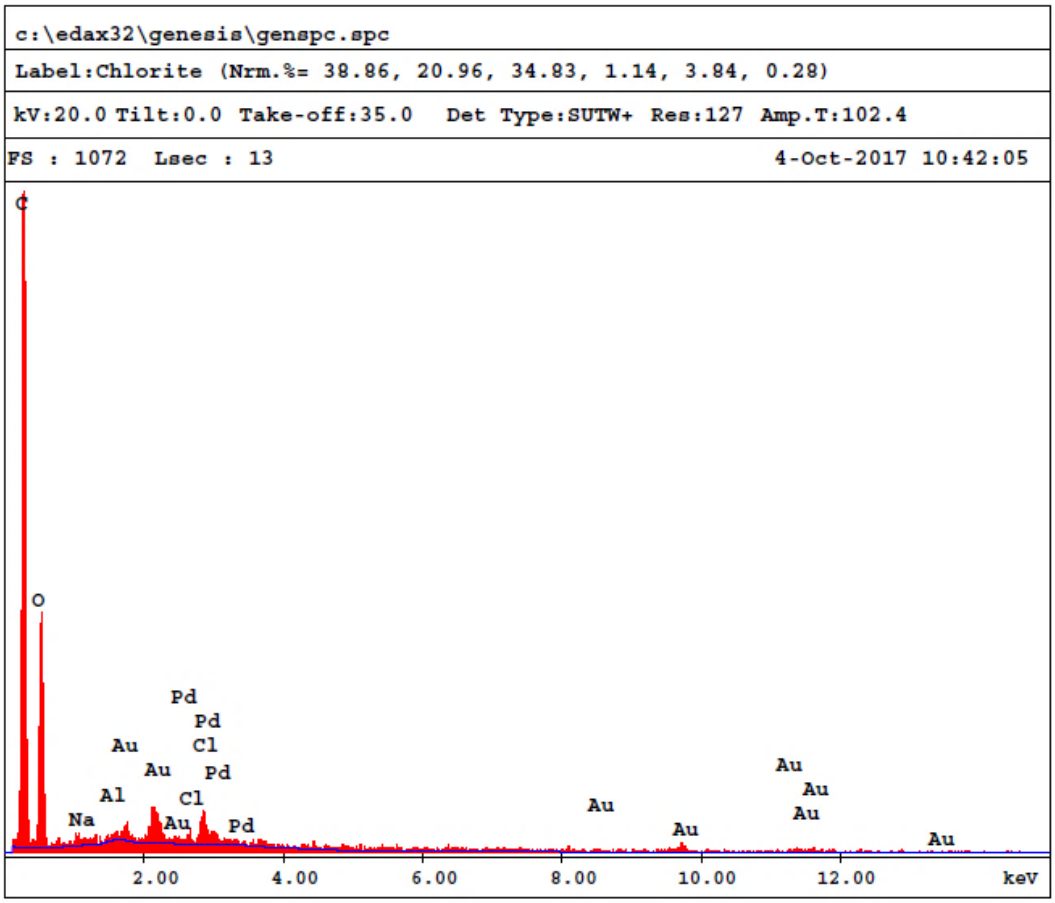

EDAX ZAF Quantification (Standardless)
Element Normalized
SEC Table : Default

Element	Wt %	At %	K-Ratio	Z	A	F
C K	62.77	75.81	0.3275	1.0278	0.5076	1.0002
O K	25.11	22.76	0.0448	1.0107	0.1767	1.0000
NaK	0.40	0.25	0.0016	0.9461	0.4157	1.0001
AlK	0.09	0.05	0.0006	0.9415	0.7117	1.0004
ClK	0.32	0.13	0.0027	0.9121	0.9157	1.0029
PdL	2.58	0.35	0.0211	0.7639	1.0735	1.0000
AuL	8.73	0.64	0.0572	0.6304	1.0387	1.0000
Total	100.00	100.00				

Figure 0.11. EDX analysis of the cross-section of the entire thickness of the supercritical CO_2-processed at SP=20.7 MPa and ST=313 K for S_{time}=24 hours VR=10.94 MPa/min of neat P_LLA films

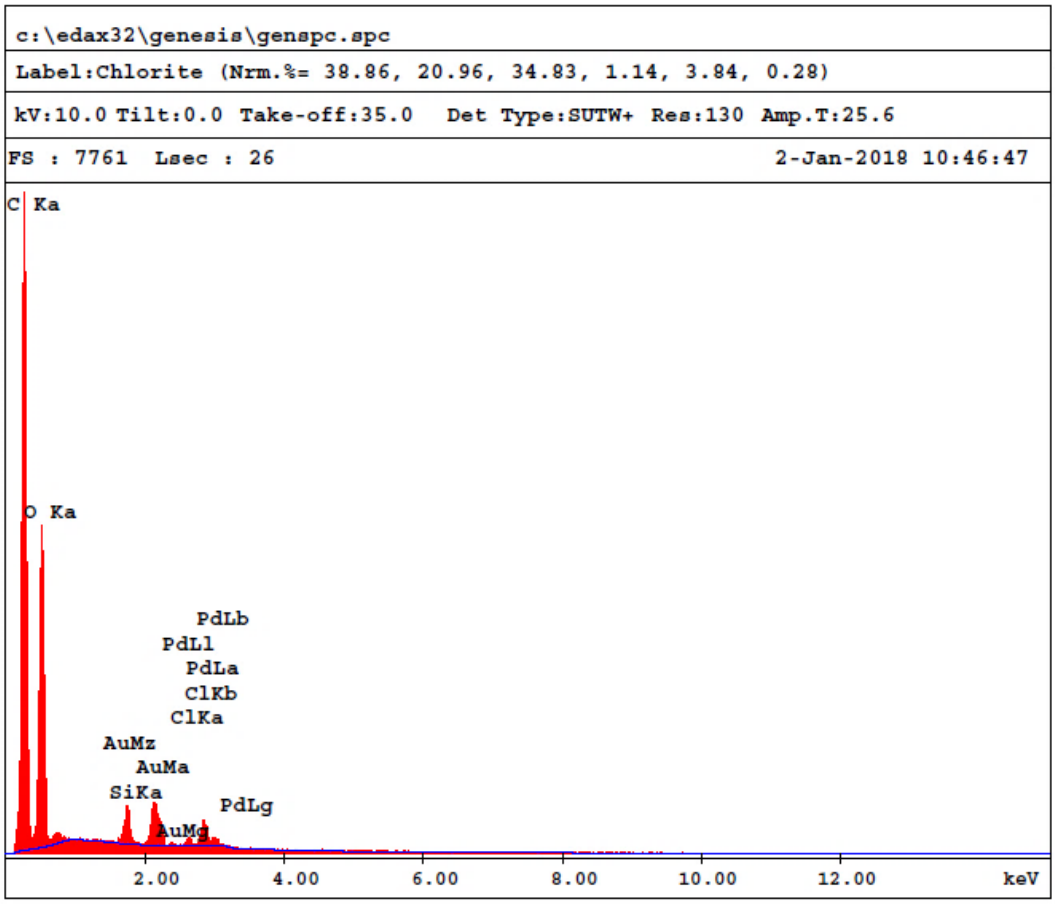

EDAX ZAF Quantification (Standardless)
Element Normalized
SEC Table : Default

Element	Wt %	At %	K-Ratio	Z	A	F
C K	55.64	72.54	0.3670	1.0539	0.6258	1.0002
O K	24.76	24.23	0.0958	1.0302	0.3755	1.0000
SiK	2.05	1.14	0.0187	0.9715	0.9372	1.0011
AuM	10.22	0.81	0.0725	0.6449	1.1000	1.0001
ClK	0.63	0.28	0.0056	0.9143	0.9669	1.0049
PdL	6.70	0.99	0.0495	0.7272	1.0167	1.0000
Total	100.00	100.00				

Figure 0.12. EDX analysis of the cross-section of the entire thickness of the unprocessed MP_LLA films

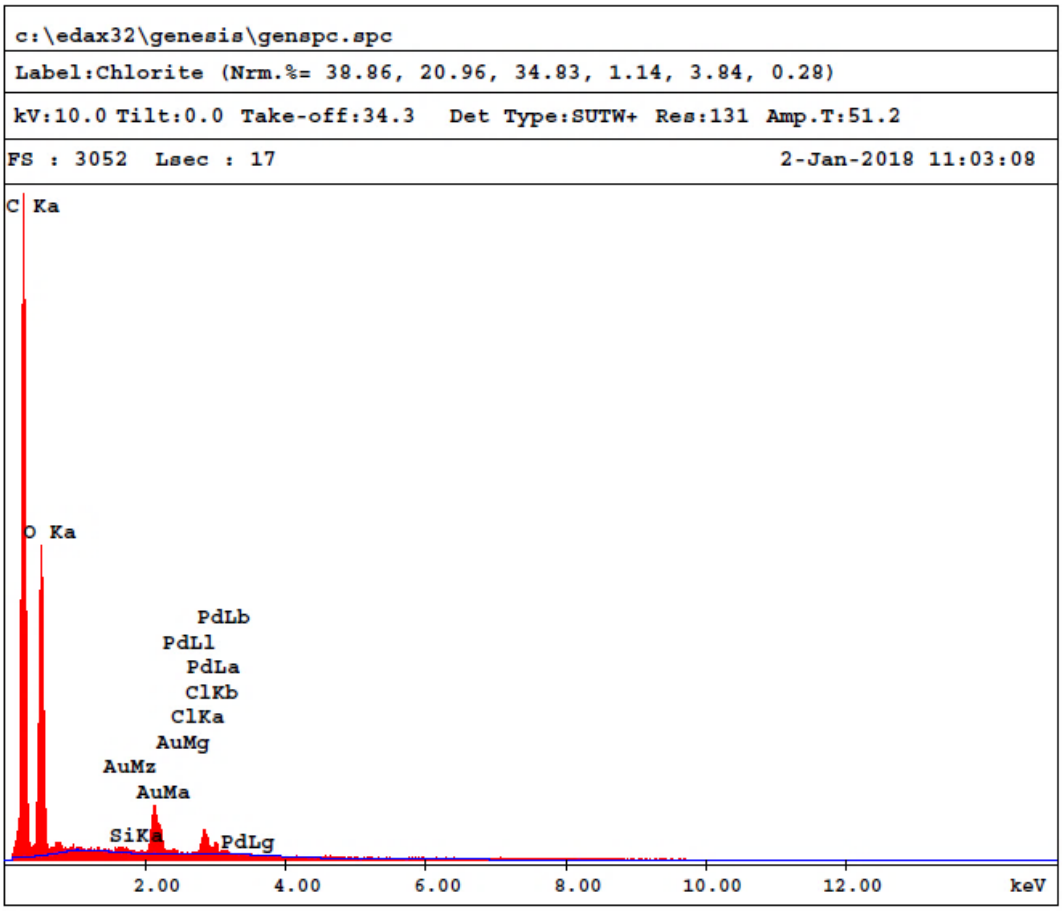

EDAX ZAF Quantification (Standardless)
Element Normalized
SEC Table : Default

Element	Wt %	At %	K-Ratio	Z	A	F
C K	55.25	72.13	0.3976	1.0557	0.6817	1.0002
O K	26.38	25.85	0.1019	1.0319	0.3745	1.0000
SiK	0.16	0.09	0.0015	0.9732	0.9326	1.0010
AuM	11.15	0.89	0.0797	0.6460	1.1062	1.0001
ClK	0.00	0.00	0.0000	0.9160	0.9662	1.0052
PdL	7.07	1.04	0.0524	0.7286	1.0177	1.0000
Total	100.00	100.00				

Figure 0.13. EDX analysis of the cross-section of the entire thickness of the supercritical CO_2-processed at SP=20.7 MPa and ST=313 K for S_{time}=24 hours VR=10.94 MPa/min of MP_LLA films

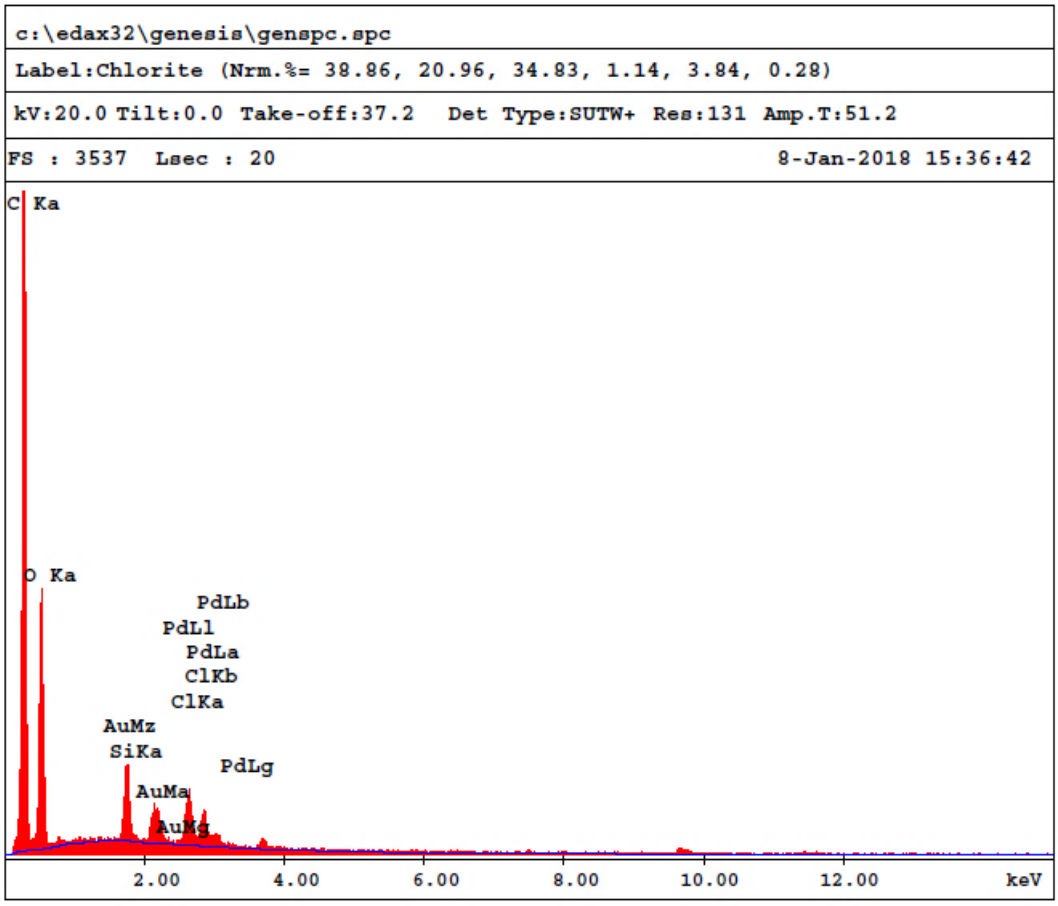

EDAX ZAF Quantification (Standardless)
Element Normalized
SEC Table : Default

Element	Wt %	At %	K-Ratio	Z	A	F
C K	65.15	75.69	0.3039	1.0186	0.4579	1.0002
O K	25.45	22.20	0.0456	1.0016	0.1788	1.0000
SiK	1.78	0.89	0.0147	0.9606	0.8553	1.0014
AuM	3.46	0.24	0.0307	0.6729	1.3174	1.0002
ClK	1.67	0.66	0.0146	0.9014	0.9624	1.0035
PdL	2.48	0.33	0.0209	0.7556	1.1120	1.0000
Total	100.00	100.00				

Figure 0.14. EDX analysis of the cross-section of the entire thickness of the unprocessed IP_LLA films

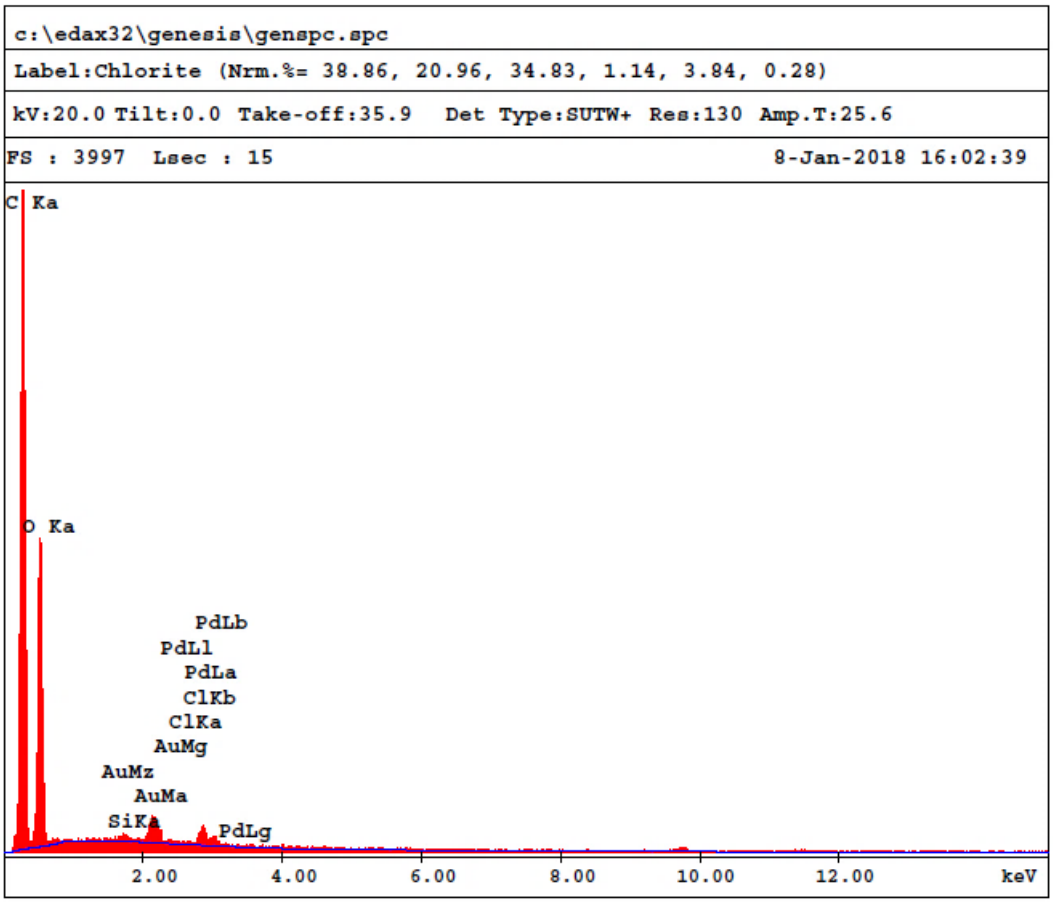

EDAX ZAF Quantification (Standardless)
Element Normalized
SEC Table : Default

Element	Wt %	At %	K-Ratio	Z	A	F
C K	61.43	70.35	0.3648	1.0145	0.5852	1.0003
O K	33.87	29.12	0.0658	0.9976	0.1949	1.0000
SiK	0.19	0.09	0.0015	0.9568	0.8391	1.0005
AuM	2.75	0.19	0.0247	0.6696	1.3398	1.0000
ClK	0.06	0.02	0.0006	0.8970	0.9735	1.0027
PdL	1.69	0.22	0.0145	0.7521	1.1428	1.0000
Total	100.00	100.00				

Figure 0.15. EDX analysis of the cross-section of the entire thickness of the supercritical CO2-processed at SP=20.7 MPa and ST=313 K for S_{time}=24 hours VR=10.94 MPa/min of IP_LLA films